

**2D FROZEN SPIN METHOD OF SEARCHING
FOR THE DEUTERON EDM IN A STORAGE RING**

by

ALEXANDER AKSENTEV

A Dissertation
Submitted to the department of electrophysical facilities
National Research Nuclear University “MEPhI”
in partial fulfillment of the requirements
for the degree of

Physics - Doctor of Philosophy

2019

Глава 1

Universal SR EDM measurement problems and their solutions

Universal SR EDM measurement problems can be classified into two groups: (i) problems that can be solved by introducing a spin wheel, and (ii) problems needing specialized solutions.

Problems of the first category follow from the instability of the invariant spin axis. Among those are, for example, local electromagnetic field perturbations, as well as perturbations to the particle spin dynamics caused by betatron oscillations. In both cases the particle invariant spin axis deviates from its equilibrium (closed orbit) orientation for a short period of time.

Problems needing specific solutions include spin decoherence and EDM-faking MDM spin precession. In this part we analyze the essence of each of these problems, describe their possible solutions, and perform corresponding simulations.

1.1 Perturbations to the spin dynamics

Problem statement

The invariant spin axis of a particle involved in betatron oscillations wobbles about its reference orientation. [1, p. 11] For this reason, the amplitude of

the T-BMT equation solution for the vertical spin vector component:

$$\begin{aligned} s_y &= \sqrt{\left(\frac{\omega_y \omega_z}{\omega}\right)^2 + \left(\frac{\omega_x}{\omega}\right)^2} \cdot \sin(\omega \cdot t + \phi) \\ &= \sqrt{(\bar{n}_y \bar{n}_z)^2 + \bar{n}_x^2} \cdot \sin(2\pi \cdot \nu_s \cdot n_{turn} + \phi), \end{aligned} \quad (1.1)$$

becomes a time-varying function. If a particle's invariant spin axis (as well as spin tune) varies in a sufficiently big range, use of a constant parameter harmonic function as a model for fitting the measured signal will introduce the model specification systematic error. Errors of this type reflect on the validity of the model parameter estimates, i.e. the frequency estimate, and hence require analysis.

Spin tune (ν_s) variability is especially problematic in this respect, since it directly affects the phase of the signal; however, this problem can be solved by introducing sextupole field elements into the beamlir, as is described in section 1.2. For this reason, we will focus on the variation of \bar{n} in this section.

Simulation

The simulation setup was as follows: a particle offset from the reference orbit in the vertical direction by 0.3 mm, is injected multiple times into an imperfect FS-type lattice [2], in which we suppress spin decoherence caused by vertical plane betatron oscillations (see section 1.2) by using the corresponding sextupole family. Machine imperfections are simulated as E+B element tilts about the optic axis. Imperfections introduced this ways do not perturb the closed orbit (that is, the reference orbit — as well as the orbit of the betatron-oscillating particle — is the same for every injection.)

Each trial, E+B element tilts are randomly distributed as $\alpha \sim N(\mu_i, 3 \cdot 10^{-4})$ degrees, $i \in \{1, \dots, 11\}$, where μ_i varies in the range $[-1.5 \cdot 10^{-4}, +2.5 \cdot 10^{-4}]$ degrees. Non-zero expectation μ_i simulated the introduction of a spin wheel driver into the beamline. [3] Magnitudes of μ_i and σ_α were picked for better detailization of the effect. At bigger values, it is more difficult to distinguish the ν_s and \bar{n} variation effects.

Another aspect of the simulation worth mentioning is that the particle injection energy of 270 MeV, which is not exactly the FS energy for this lattice (270.0092 MeV is the most precise value we could obtain). Because of this the invariant spin axis \bar{n} points mostly in the vertical direction (deviating from it by no more than 51° at higher spin wheel roll rates); its radial component (determining the spin vector's vertical component's oscillation amplitude) is relatively small, and hence the more sensitive to perturbations caused by the betatron motion.

Spin tracking was done in COSY Infinity [4], for $1.2 \cdot 10^6$ beam revolutions; every 800 revolutions ν_s and \bar{n} were computed (using procedure TSS [5, p. 41]) at the phase space point occupied by the particle at the moment, which gives us the first data set $(\nu_s(n), \bar{n}(n))$, n being the revolution number. The corresponding spin vector components $(s_x^{trk}(n), s_y^{trk}(n), s_z^{trk}(n))$, computed by the tracker (procedure TR [5, p. 41]), make up the second set of data series used in the analysis.

Analysis

Using the first data set we computed the expected $s_y^{gen}(t)$ “generator” time series, according to equation (1.1), as well as the “ideal” series s_y^{idl} , in which we assumed constant values $\nu_s = \langle \nu_s(t) \rangle$ and $\bar{n} = \langle \bar{n}(t) \rangle$.

Our hypothesis is that the betatron motion will introduce a discrepancy between the ideal harmonic model

$$f(t) = a \cdot \sin(\omega \cdot t + \delta), \quad (1.2)$$

and the tracker data, by varying the spin precession axis \bar{n} , and hence the amplitude of the fitted signal. The “ideal” series serves as the basis for analysis, since it perfectly corresponds to the regression model; the “generator” series accounts for the variation of \bar{n} , while still remaining within the bounds of the regression model. The “tracker” series is our closest approximation to the real measurement data.

In order to cross-compare the series, we *a*) computed and analyzed the residuals $\epsilon_1(t) = s_y^{gen}(t) - s_y^{idl}(t)$ and $\epsilon_2(t) = s_y^{trk}(t) - s_y^{idl}(t)$; *b*) fitted

model (1.2) to the three time series and compared the fit quality; *c*) computed the standard deviations of the \bar{n} components at different spin wheel roll rates.

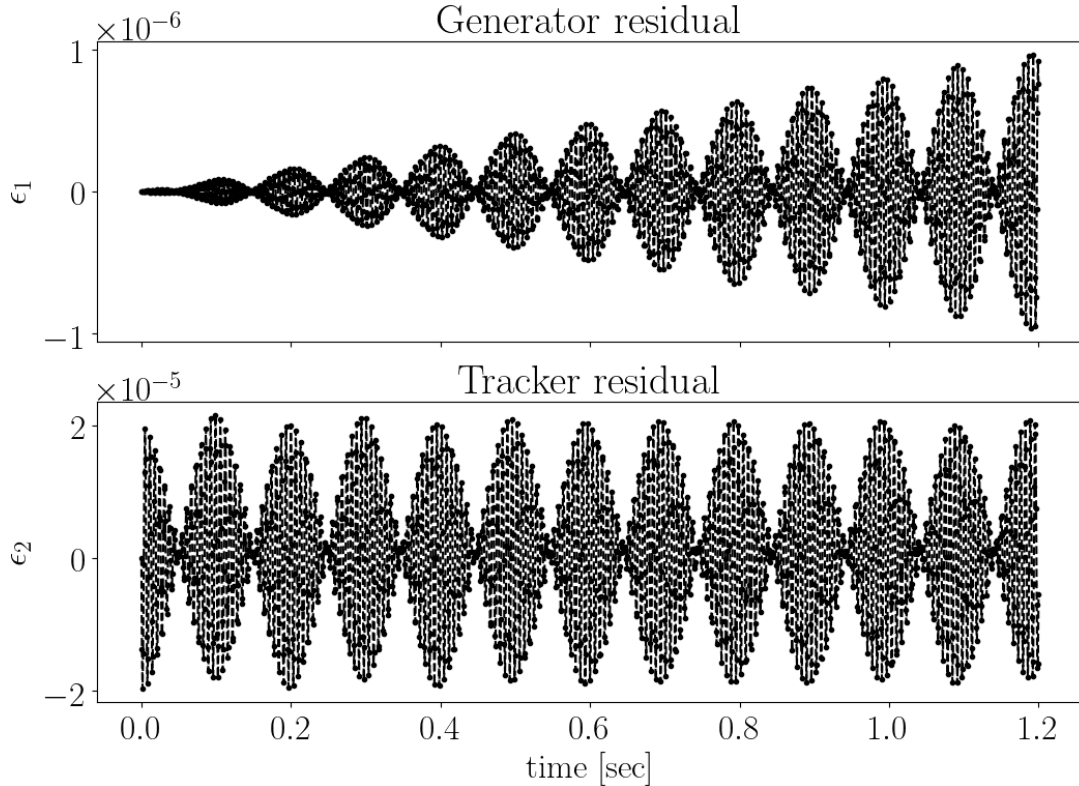


Рис. 1.1: Comparator residuals as functions of time. Top panel: ϵ_1 residual; bottom panel: ϵ_2 residual

In Figure 1.1 we observe that the “generator” is almost identical to the “ideal” series, with $\epsilon_1 \leq 1 \cdot 10^{-6}$ (even though its oscillation frequency is slightly off) for the duration of the cycle, while the “tracker” series deviates from it at the level $\epsilon_2 \leq 2 \cdot 10^{-5}$. The discrepancy between ϵ_1 and ϵ_2 is observed systematically at all spin wheel roll rates (see Figure 1.2b), and does not have an explanation so far.

In Figure 1.2b we see that the standard deviations of both residuals exhibit the same dependence on the spin wheel roll rate as that of ν_s (Figure 1.2a, bottom panel), but show indifference toward the behavior of \bar{n} . This is an indication that frequency variation contributes a great deal more to the

Таблица 1.1: Model parameter estimates (slow SW)

Series	Par.	Value	St.Err	AIC
s_y^{idl}	\hat{f}	4.220359687911	$6.9 \cdot 10^{-11}$	
	\hat{a}	0.12514597851	$4 \cdot 10^{-11}$	-62093
	$\hat{\delta}$	$-1.50 \cdot 10^{-8}$	$4 \cdot 10^{-10}$	
s_y^{gen}	\hat{f}	4.2203596911	$1.9 \cdot 10^{-9}$	
	\hat{a}	0.125145979	$1 \cdot 10^{-9}$	-52142
	$\hat{\delta}$	$-1.6 \cdot 10^{-8}$	$1.2 \cdot 10^{-8}$	
s_y^{trk}	\hat{f}	4.2203603	$1.3 \cdot 10^{-6}$	
	\hat{a}	0.12514597	$3.7 \cdot 10^{-7}$	-34567
	$\hat{\delta}$	$-4 \cdot 10^{-6}$	$6 \cdot 10^{-6}$	

discrepancy between model (1.2) and the tracker data than the presumed amplitude variation caused by the wobbling of \bar{n} during betatron oscillations.

Table 1.1 characterized the model fit quality with respect to the used data set at the slowest spin wheel roll rate. We observe that the cross-differences between the parameter estimates at different time series are not statistically significant. Even though the variation of the spin precession angular velocity degraded the fit quality, it did not introduce any statistically-significant bias into the estimates.

Conclusions

The question of the influence of betatron motion on the EDM statistic in the FD method should be considered in view of three circumstances:

- (a) The signal amplitude oscillations (as estimated by ϵ_2) are small. They occur at the 10^{-4} level (when $\alpha \sim N(0, 3 \cdot 10^{-2})$ degrees), whereas the expected polarization measurement error is on the order of percents. This means the superposition of this systematic error with the random measurement error will exhibit no statistically-significant systematicity.

- (b) The correlation coefficient between the amplitude and frequency estimates is not significant. The amplitude oscillations affect the \hat{a} -estimate foremost; their effect on the $\hat{\omega}$ -estimate is secondary, and is described by the correlation coefficient. Since it is less than 10%, even if the oscillations happen to be strong enough to affect the amplitude estimate, their effect on the frequency estimate will be reduced by at least a factor of 10.
- (c) This systematic effect is controllable. And this point is the major advantage of the FD methodology. By applying an external Spin Wheel, the \bar{n} oscillations can be continuously minimized as much as necessary, without changing the experiment pattern.

1.2 Spin decoherence

Spin coherence refers to a measure or quality of preservation of polarization in an initially fully-polarized beam. [6, ctp. 205]

The spin vectors of a polarized beam injected into a storage ring begin precessing about the vertical (guiding) field. The precession frequency depends on the particle equilibrium energy level, which differs across the beam particles.

This circumstance doesn't pose a problem when the beam is vertically polarized; however, the FS SR EDM measurement method requires that the polarization vector be aligned with the beam's momentum vector, i.e. lay in the horizontal plane. Hence, spin decoherence is an inherent problem of the FS methodology.

In the present section we analyze the origins of spin decoherence, the sextupole method of its suppression, as well as the simulation results proving the effectiveness of the method.

As an introduction, though, we estimate the spin coherence time required for the measurement of the EDM in the framework of the space domain methodology.

Spin coherence time requirements

Operating in the space domain FS methodological framework in a perfectly-aligned lattice,¹ the spin coherence time (SCT) is determined by the minimal detectable angle by which the polarization vector deviates from the beam orbit plane as a result of the EDM action alone. For the sensitivity level of $10^{-29} e \cdot cm$ this angle is approximately $5 \cdot 10^{-6}$. [7]

According to the T-BMT equation,

$$\Omega_{EDM,x} = \eta \frac{qE_x}{2mc},$$

where η is the proportionality coefficient between the EDM and spin, in the deuteron case equal to 10^{-15} , for the given sensitivity level. [6, p. 206]

For the deuteron BNL FS ring, $E_x = 12$ MV/m, [7, p. 19] therefore $\Omega_{EDM,x} \approx 10^{-9}$ rad/sec. Hence we obtain that, in order to reach a detectable level of at least 1 μ rad one needs an SCT on the order of 1,000 seconds. [6, p. 207]

Origins of decoherence

Spin decoherence in a particle beam results from the dispersion of the beam particles' spin precession angular velocities, which, in its turn, is a result of the difference between their orbit lengths and initial momenta. The orbit length effect on the particle spin tune is described by the concept of the effective Lorentz-factor, which was introduced in section ??.

From equations (??) for spin tune in electrostatic and magnetic fields it follows that the spin tunes of two particles having equal values of the effective L-factor are equal, regardless of their trajectories in the accelerator. This principle is the basis for the proposed sextupole field spin precession suppression theory, as well as the procedure for flipping the polarity of the storage ring's guide field, which is required for injecting the deuteron beam in the opposite direction in order to cancel the EDM-faking MDM spin precession.

¹In fact, perfect element alignment is a pre-requirement of the space domain.

Sextupole field spin decoherence suppression theory

In order to minimize spin decoherence related to particle betatron motion and momentum spread sextupole (or octupole) fields can be used. [6, p. 212]

A sextupole of strength

$$S_{sext} = \frac{1}{B\rho} \frac{\partial^2 B_y}{\partial x^2},$$

where $B\rho$ is the magnetic rigidity, modifies the first-order momentum compaction factor as [8, p. 2581]

$$\Delta\alpha_{1,sext} = -\frac{S_{sext} D_0^3}{L}, \quad (1.3)$$

and simultaneously the orbit length as

$$\left(\frac{\Delta L}{L}\right)_{sext} = \mp \frac{S_{sext} D_0 \beta_{x,y} \varepsilon_{x,y}}{L}, \quad (1.4)$$

where $D(s, \delta) = D_0(s) + D_1(s)\delta$ denotes the dispersion function.

One can formulate the principle of the sextupole field effect in the following way. A particle in an accelerator does performs betatron oscillations about some closed orbit. Due to dispersion, the closed orbit is different for different particles in the beam. A sextupole field works like a prism, focusing (or defocusing) the particles' closed orbits.

In the next sections we will call the decoherence associated with the horizontal/vertical betatron oscillations, respectively synchrotron oscillations, the X-/Y-, and D-decoherence. Sextupole families aimed at reducing X-, Y-, and D-decoherence will be denoted, respectively, GSX, GSY, GSD.

From equations (1.3), and (1.4) one can see that one needs to use three sextupole families, placed respectively in the maxima of the β_x , β_y (for the X-, Y-types), and D_0 (for the D-type) functions, in order to suppress spin decoherence in the beam.

Simulation in an ideal ring

In order to check the capability of the sextupole field spin decoherence suppression method we carried out a simulation in which we used the FS-type lattice described in section ???. Since the lattice is perfectly aligned, spin precession occurs only about the vertical (\hat{y}) axis.

SCT optimization is done at 270.00 MeV energy, the orbital and spin transfer matrices of the lattice are computed up to the fifth order of the Taylor expansion.

Three sextupole families are used, to suppress the X, Y-, and D-type decoherence respectively. Each sextupole family's field gradient is optimized separately (the gradients of the other two families are set to zero). We optimize the sextupoles separately because otherwise we run into a numerical problem with the TSS procedure.²

The sextupole field optimization procedure is as follows. First, the lattice's transfer matrices are computed at the given sextupole gradient strength. Then, using procedure TSS we compute the spin tune and invariant spin axis (ISA) Taylor expansions. Depending on the optimized family, we pick the coefficient at the square of the corresponding phase space variable (x , y , or δ) from the spin tune Taylor expansion. The absolute value of the coefficient is used as the objective function: i.e., at the optimal gradient, does not depend (parabolically) on the corresponding particle offset from the reference one.

The Simplex algorithm was used for optimization. [9, p. 37]

In Figure 1.3 the spin tune dependence on the particle offset from reference in three phase space coordinate before and after turning on the relevant sextupoles. One can see that in all three cases the parabolic dependence has been suppressed. However, there remains a linear dependence, which is insensitive to the sextupole fields. The linear dependence is observed when modeling the spin dynamics in the codes COSY INFINITY, MODE, as well

²We also studied the possibility of finding the optimal set of gradient values, by directly computing the relevant spin tune Taylor expansion coefficients in the 3D gradient space mesh. The question needs further investigation, but at this point we doubt that all three families can be optimized simultaneously. This could be the reason why in [6, p. 219] only two sextupole families are used in the lattice codenamed BNL.

as MAD (from private communication with Y. Senichev). Based on that, one can hypothesize that the linear term is not a numerical artifact of COSY INFINITY, but rather has a physical basis. This question needs further consideration, but at this point it is thought that this term can be suppressed by adjusting the RF cavity parameters. [6, p. 210, 219]

Transfer of decoherence into the vertical plane in an imperfect lattice

We injected an ensemble of 30 particles, uniformly distributed along the vertical axis in the range $y \in [-1, +1]$ mm, into an imperfect FS lattice. Since the analysis is based only on the tracker data, and does not involve the TSS procedure, the beam was injected at the exact FS energy 270.0092 MeV.

Imperfections are simulated by E+b element tilts about the optic axis by angles picked from the normal distribution $\Theta_{tilt} \sim N(0, 1 \cdot 10^{-4})$ radians. Since such imperfections conserve the Lorentz force, they do not perturb the particle orbital dynamics and affect only the spin dynamics. The magnitude of the standard deviation reflects the realistic element alignment precision.

In Figure 1.4 we show the standard deviation of the radial components of the ensemble's spin vectors before and after turning on the sextupoles. Since the particles move in an imperfect lattice, their spin vectors rapidly turn in the vertical plane, and hence σ_{s_x} is a rapidly oscillating function exhibiting no long-term growth trend (the slope of the trend line is $(2 \pm 2) \cdot 10^{-8}$ 1/sec). This means there's no spin decoherence in the horizontal plane. When the sextupoles are turned on the σ_{s_x} amplitude is reduced by a factor of 10.

In Figure 1.5 is shown the same statistic for the vertical spin vector components. A long-term trend is observed (the slope is $(4.5 \pm 0.6) \cdot 10^{-7}$ 1/sec) prior to turning on the correcting sextupoles. The sextupole correction does not reduce the oscillation amplitude, but suppresses the accumulation of dispersion (the slope drops to $(5 \pm 6) \cdot 10^{-8}$ 1/sec).

Analysis of spin decoherence in an imperfect lattice

The following tests were done with a planar bunch of 30 particles injected into a FS lattice with E+B elements tilted about the optic axis by angles picked from $N(0, 5 \cdot 10^{-4})$ radians.

The beam particles were normally-distributed in the vertical plane $y - z$ along the \hat{y} -axis as $y \sim N(y_0, 0.1)$ mm (all other phase space coordinates are zero). The offset y_0 varied in the range $[-1, +1]$ mm. Initially all particles' spins were longitudinally oriented $\mathbf{S}(t = 0) = (0, 0, 1)$.

We also varied the value G_Y of the GSY sextupole. G_Y varied in the range $[G_Y^0 - 5 \cdot 10^{-3}, G_Y^0 + 5 \cdot 10^{-3}]$, where $G_Y^0 = -5.77 \cdot 10^{-4}$ is the optimal gradient for this particular imperfection distribution. The value G_Y^0 was found by minimizing the coefficient a_2 of the Taylor expansion $\nu_s(y) \approx a_0 + a_1 \cdot y + a_2 \cdot y^2 + O(y^3)$.

There were 10 injections at each value of G_Y .

To ensure the stability of the TSS procedure of COSY Infinity [5], the beam was injected at 270 MeV (the strict FS occurs at 270.0092 MeV), and the orbital and spin transfer matrices were built up to the third order Taylor expansion.

After that the beam is tracked through the lattice for $1.2 \cdot 10^6$ turns, which is approximately equivalent to 1.2 seconds. Data used in the analysis were collected every 800 turns.

What we collected: *a*) TSS procedure results: spin tune (ν_s) and the ISA (\bar{n}) components, и *b*) spin (S_X, S_Y, S_Z) and phase space (X, A, Y, B, T, D) vector components. We also recorded the Taylor expansions of ν_s , \bar{n} , orbital, and spin transfer matrices of the lattice at each G_Y value.

From the spin vector component data we computed the ensemble polarization:

$$\mathbf{P} = \frac{\sum_i \mathbf{s}_i}{|\sum_i \mathbf{s}_i|}. \quad (1.5)$$

Its vertical component is fitted by $f(t; a, f, \phi) = a \cdot \sin(2\pi \cdot f \cdot t + \phi)$, where all three parameters $(\hat{a}, \hat{f}, \hat{\phi})$ are estimated.

Sextupole field effect on spin tune and invariant spin axis

In Figure 1.6 we showed the dependence of spin tune on the particle's vertical offset from the reference orbit: $\nu_s(y) \approx a_0 + a_1 \cdot y + a_2 \cdot y^2 + O(y^3)$. In Figure 1.6a one can observe the unbending of the parabola when $G_Y \rightarrow G_Y^0$.

An equivalent dependence for the vertical component of the ISA is shown in Figure 1.7. In Figure 1.7a we observe that the ISA component behaves the same way as spin tune when $G_Y \rightarrow G_Y^0$. Just as in the case of an ideal lattice, in Figure 1.7b one can observe the presence of a linear term in $\bar{n}_y(y)$, insensitive to the sextupole fields.

In the figures above, the values of spin tune and ISA were computed as univariate functions of the vertical offset; all other phase space coordinates were set to reference values. While analyzing the tracker data we noted that the ISA components (as well as spin tune) of a particle do not oscillate, as one would expect from the figures, but remain nearly constant. We hypothesized that the ν_s and \bar{n} dependencies on the vertical offset and its derivative ($y' \equiv a$) compensate each other when the particle moves along a real trajectory. On the next figures we depicted ν_s , \bar{n} at their true phase space trajectories in the storage ring.

In Figure 1.8 are depicted the particle trajectories in the (Y, B) phase plane, obtained in tracking the particles through the imperfect lattice.

In Figures 1.9, 1.10, 1.11, and 1.12 are plotted, respectively: spin tune, the radial, vertical, and longitudinal components of the ISA, computed at the trajectories plotted in Figure 1.8, in two cases: *i*) sextupoles are turned off, and *ii*) GSY sextupoles are turned on.

From the analysis of the figures, we can gather the following:

- (a) in the sextupoles-off case, both ν_s and the direction of \bar{n} are mostly (to the linear Taylor expansion term) fixed by the value of the particle's transverse emittance;
- (b) in the sextupoles-on case, the mean levels of ν_s and \bar{n} of different particles come together, and the betatron motion effect, related to the presence of a linear Taylor expansion term, becomes apparent.

Hence, Figures 1.10 and 1.11 are evidence that not only are the **frequencies** but also the **directions** of the beam particles' spin precession angular velocity vectors are equalized when sextupole fields are used to suppress spin decoherence. The longitudinal component of the ISA is insensitive to the sextupole fields, as evidenced by Figure 1.12.

In Figure 1.13 are shown the dependencies of the radial and vertical ISA components' mean levels on the particle's mean spin tune level. Based on this figure, we conclude in section 1.5 that particles having equal effective Lorentz factor values are equivalent in terms of their spin dynamics in the general (direction and magnitude of the spin precession angular velocity vector) sense.³

Analysis of the sextupole spin decoherence suppression mechanism

From equations (??) and (??), the dependence of spin tune of the particle equilibrium energy can be expressed as:

$$\nu_s = G\gamma_0 + G \frac{\gamma_0^2 - 1}{\gamma_0} \cdot C_0 \cdot f_1(\epsilon_x, \epsilon_y, Q_x, Q_y) + G \frac{\gamma_0^2 - 1}{\gamma_0} \cdot C_0 \cdot f_2(\alpha_1, \langle \Delta K/K \rangle^2),$$

where C_0 is a constant, f_1 and f_2 are defined in equation (??).

Since a betatron-oscillating particle does also synchrotron oscillations, the effect of sextupole fields on it is a superposition of effects. A particle injected onto the reference orbit, but having an initial energy offset, does only synchrotron oscillations. Consequently, sextupole fields affect its spin tune by only modifying the momentum compaction factor, i.e. f_2 .

In view of that, we carried out a simulation in which we consecutively injected two beams of 30 particles: in the first one, the D-bunch, particles were distributed as $\delta \sim N(0, 0.5 \cdot 10^{-6})$, in the second one, the Y-bunch, as $y \sim N(0, 0.5)$ mm. All the other phase space coordinates were initially set to zero.

³At least this seems to be true when operating in the frozen spin regime.

The bunches were injected into the ideal FS lattice in order to exclude effects associated with perturbations of non-reference orbits. For the D-bunch, only the GSD sextupoles were turned on; for the Y-bunch – GSY. The sextupole gradients were varied $\pm 5 \cdot 10^{-3}$ of the corresponding family's optimal gradient value.

Spin tracking was done for $1.2 \cdot 10^6$ turns, data were recorded every 800 turns.

In Figure 1.14 are plotted the particles' longitudinal phase space portraits. We see that the D-bunch phase portraits are practically all centered at the same point,⁴ and that their emittances do not change when the sextupole strength is varied.

At the same time, the Y-bunch phase portraits vary with the sextupole field strength. We observe that the ellipse centers (i.e. the equilibrium energy levels) are the most compressed at a gradient value that is **not** optimal (the phase portraits for the latter are drawn in the middle panel). This observation was what motivated us to try to inject the D-bunch in the first place. We explain this observation by the superposition of the orbit length and momentum compaction factor effects.

For a more thorough analysis of the sextupole field effects on the functions f_1 and f_2 we plotted the dependencies of the particles' mean spin tune levels on their equilibrium energy levels at different sextupole field strengths (Figure 1.15). One can see from the figure that the point distribution density in the D-bunch plot does not vary with the gradient value; the only thing that changes is the functional dependence of spin tune on the equilibrium energy level, as is expected from the functional form of f_2 (cf. section ??). Hence, the signature of the sextupole field's momentum compaction effect is the change in the functional form of $\langle \nu_s \rangle = f(\langle \Delta K / K \rangle)$.

In the Y-bunch plot one observes two effects: both the point distribution density (i.e. the beam's longitudinal emittance) and the functional form of $\langle \nu_s \rangle(\langle \Delta K / K \rangle)$ change.

⁴When zooming in, one can see that the ellipse centers are slightly different, but this difference is insensitive to the sextupole gradient value, and most likely is the result of finite statistics.

Conclusion: The simulation confirms statements (1.3) and (1.4).

1.3 Ошибки неидеальности ускорителя

Systematic errors due to physical imperfections of the accelerator lattice, including optical element misalignments, are causative to an EDM-faking signal related to MDM spin precession [6, з. 230] Rotational magnet misalignments are particularly problematic in this respect, since they induce parasitic horizontal magnetic field components B_x and B_z , both of which precess spin in the vertical plane; the one in which the EDM is searched for.

Y. Senichev made analytical estimates [10] of the radial component of the spin precession angular velocity vector. From the T-BMT equation, and the expression for the Lorentz force, the radial component can be expressed as

$$\sigma [\Omega_x^{MDM}] = \frac{q}{m\gamma} \frac{G+1}{\gamma} \frac{\sigma [B_x]}{\sqrt{n}}, \quad (1.6)$$

where n is the number of tilted spin-rotator elements,⁵ and $\sigma [B_x] = B_y \sigma [\delta h] / L$, with the misalignment error standard deviation $\sigma [\delta h]$. Assuming $\sigma [\delta h] = 100 \mu\text{m}$, and the spin-rotator length $L = 1 \text{ m}$, $\sigma [\Omega_x^{MDM}] \approx 100 \text{ rad/sec}$. [10]

We analyzed the particle spin dynamics in the imperfect FS and QFS lattices using the COSY Infinity code. Our simulation results tend to confirm the above estimates.

Imperfection field implementation When implementing the machine imperfections we followed recommendations given in [6, p. 235]. A small perturbation of the magnetic field acts like a small proportional rotation of the spin vector. For this reason we implemented the E+B element tilt as a product between the element's spin transfer matrix and the corresponding rotation matrix, a “spin kick.” Such an implementation guarantees the preservation of the closed orbit. This orbit preservation is physically grounded in the fact that when a spin-rotator is tilted, there emerges a compensating electric field keeping the Lorentz force constant.

⁵The estimates were made for the FS lattice described in section ??

According to equation (??), a change in the MDM precession angular velocity associated with the presence of a parasitic magnetic field $(B_x, 0, B_z)$ is

$$\Delta\Omega_{MDM} = \frac{q}{m} G \cdot (B_x, 0, B_z),$$

hence the spin kick angle

$$\Theta_{kick} = t_0 \Delta\Omega_{MDM},$$

where $t_0 = L/v_0$ is the reference particle's time of flight through the element.

Tilt distribution dependence

This series of simulations was carried out in order to prove (or reject) the validity of two theses concerning the machine imperfection systematic error: (1) the induced MDM spin precession angular velocity component is independent of the particular element tilt distribution, and depends only on the mean tilt angle; and (2) this dependence is linear.

The simulation was set up as follows: in the FS lattice described in section ?? E+B elements were randomly tilted about the optic axis by angles Θ_{tilt} . After building the third-order spin and orbital transfer maps, we computed the Taylor expansions of the spin tune and spin precession axis (SPA). The zero-order terms of the Taylor expansions represent the spin tune and SPA of the reference particle.

The reference particle spin precession angular velocity is calculated according to equation: [11, p. 4]

$$\Omega = 2\pi/\tau_0 \cdot \nu_s \cdot \bar{n},$$

where $\tau_0 = f_{rev}^{-1} = 10^{-6}$ seconds is the particle's time of flight through the full lattice.

The simulation was carried out 11 times; each time the spin-rotator tilt angles were picked from a normal distribution $N(\mu_0 \cdot (i - 5), \sigma_0)$, where $\mu_0 = 10 \cdot \sigma_0 = 10^{-4}$ rad, $i \in \{0, \dots, 10\}$. The simulation results are plotted in Figure 1.16.

One can observe from the figure that a tilt distribution at which the mean tilt angle is equal to 10^{-4} radians, the beam polarization vector precesses in the vertical plane at the rate of 500 rad/sec. This agrees with the estimates mentioned above (section 1.3), because in them a tilt error standard deviation of 10^{-4} rad is assumed at 100 tilted elements. In that case, the mean tilt angle standard deviation is 10^{-5} , and hence MDM precession occurs at a rate up to 50 rad/sec with a probability 67%, and up to 100 rad/sec with a probability 95%.

Figure 1.17 shows the results of a simulation in which six, randomly-picked E+B elements were pair-wise tilted by opposite angles, while one element was tilted by an angle $\mu_i = (i - 5) \cdot 10^{-6}$ rad, $i \in \{0, \dots, 10\}$.

Both simulations were done at the strict FS energy 270.0092 MeV.⁶ One can see that the compensated elements do not contribute to the spin precession.

Comparison of the CW vs CCW beams' spin precession angular velocities

In Figure 1.18 we plotted the relative difference between the CW and CCW beams' radial SPA/angular velocity components in the case of both the normally-distributed and mutually-compensated tilt cases.

For the radial SPA component the relative difference was computed as

$$\delta \bar{n}_x = \frac{\bar{n}_x^{CW}(\langle \Theta_{tilt} \rangle) - \bar{n}_x^{CCW}(\langle \Theta_{tilt} \rangle)}{\bar{n}_x^{CW}(\langle \Theta_{tilt} \rangle)};$$

for the angular velocity:

$$\delta \Omega_x = \frac{\Omega_x^{CW}(\langle \Theta_{tilt} \rangle) - \Omega_x^{CCW}(\langle \Theta_{tilt} \rangle)}{\Omega_x^{CW}(\langle \Theta_{tilt} \rangle)}$$

⁶At this energy, in the ideal lattice, ν_s and \bar{n} are undefined in the beam rest frame used in COSY Infinity. This corresponds to the situation when spin does not precess in any plane (either horizontal or vertical), which corresponds to the realization of the 3D FS condition in an ideal lattice.

One can observe in the figures that in both cases both beams' SPA has the same orientation; there is a difference between the beams' spin tunes, but it stays below the percent level. The spin tune difference grows bigger as the spin wheel roll rate (proportional to the mean tilt angle) gets slower. The spin tune difference may indicate that the lattice is asymmetric, with respect to the spin dynamics, relative to the beam circulation direction (i.e. time reversal). It may be explained by a difference between the CW and CCW beams' closed orbits.

1.4 Смена полярности ведущего поля

Необходимо уделить внимание двум аспектам проблемы смены полярности ведущего поля:

- (a) Какой параметр системы должен оставаться постоянным от цикла к циклу;
- (b) Как его можно наблюдать.

Целью смены полярности ведущего поля является точное воспроизведение радиальной компоненты частоты МДМ прецессии, индуцированной полями неидеальности ускорителя. Этот момент часто упускается из виду: простое воспроизведение величины магнитного поля не достаточно, поскольку точка инжекции центроида пучка, а значит его длина орбиты — и соответственно, ввиду уравнений (??) и (??), спин-тюн, — подвержена вариации. (Помимо этого, ускорительная структура может быть асимметрична, с точки зрения спиновой динамики, относительно обращения направления движения пучка.)

Таким образом, необходимо восстанавливать не величину поля, а эффективный Лоренц-фактор центроида.

Касательно второго вопроса, мы уже говорили, что скорость вращения Спин-Колеса контролируется через измерения частоты прецессии спина в горизонтальной плоскости. Эта плоскость была выбрана потому, что вектор угловой скорости ЭДМ прецессии смотрит (по большей

части) в радиальном направлении; его вертикальная компонента возникает из-за полей неидеальности ускорителя, и мала по-сравнению с их-меряемым ЭДМ эффектом. Поэтому, в первом приближении, когда мы манипулируем вертикальной компонентой совокупной угловой скорости спин-прецессии, мы манипулируем вертикальной компонентой вектора угловой скорости МДМ-прецессии.

Процедура калибровки эффективного Лоренц-фактора состоит в следующем.

1.5 Спин-тюн эквивалентность траекторий частиц с одинаковыми значениями эффективного Лоренц-фактора

В контексте процедуры смены направления вращения Спин-Колеса, важно рассмотреть вопрос эквивалентности спин-динамики CW и CCW пучков.

Отправной точкой нашего анализа является утверждение 1: частицы с одинаковым значением эффективного Лоренц-фактора имеют одинаковый спин-тюн, то есть эквивалентны с точки зрения спиновой динамики. Это следствие уравнения (??).

В следующих разделах мы проанализируем две формулировки утверждения 1:

- A. интерпретируя эффективный Лоренц-фактор как математическое ожидание кинетической энергии частицы;
- B. функция многих переменных $\nu_s(x, a, y, b, \ell, \delta)$ агностична к фазовой траектории частицы в поперечном фазовом пространстве (x, a) , и (y, b) , т.е. может быть сведена к функции одной переменной $\nu_s(\gamma_{eff})$.

Формулировка А

Формулировка В

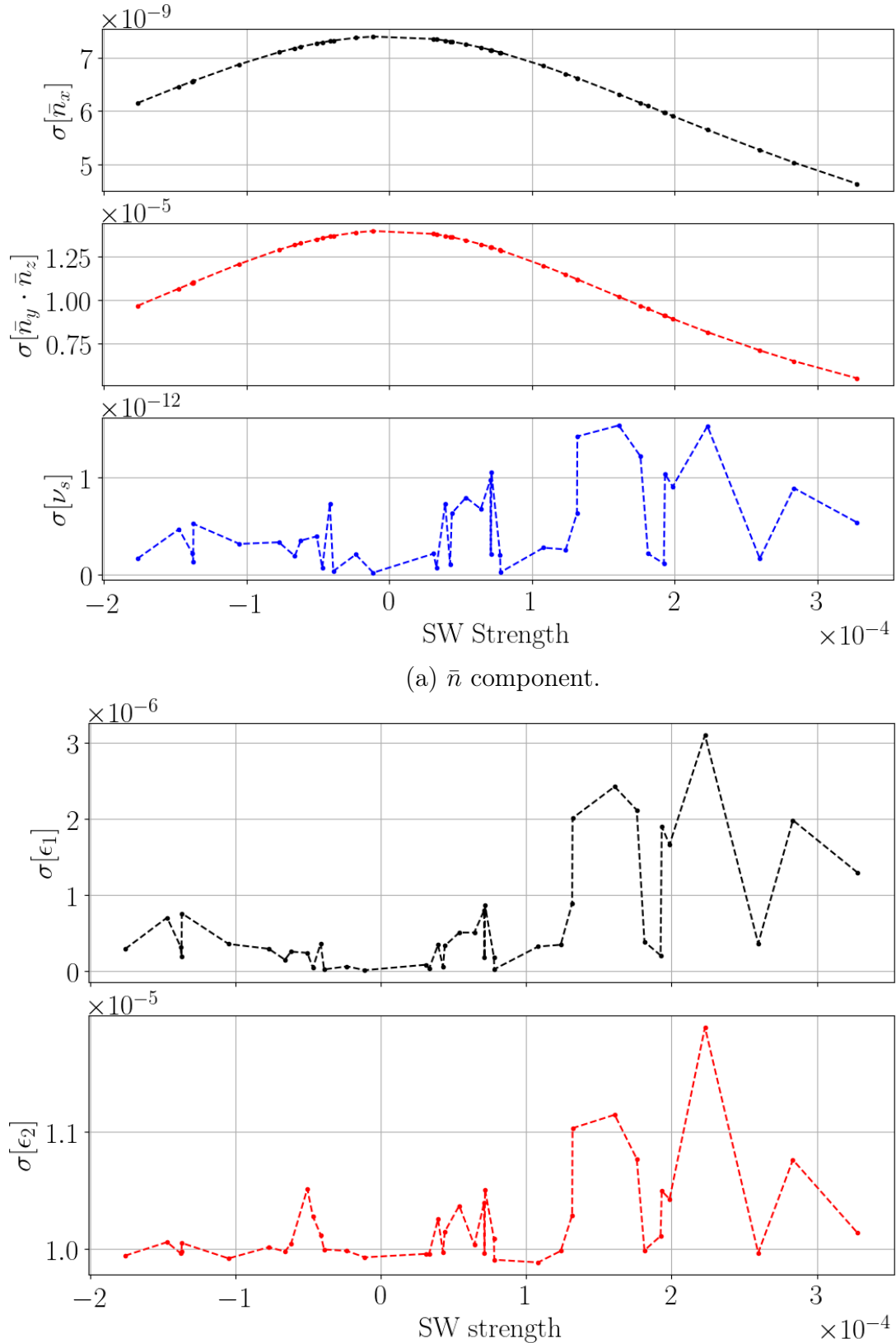
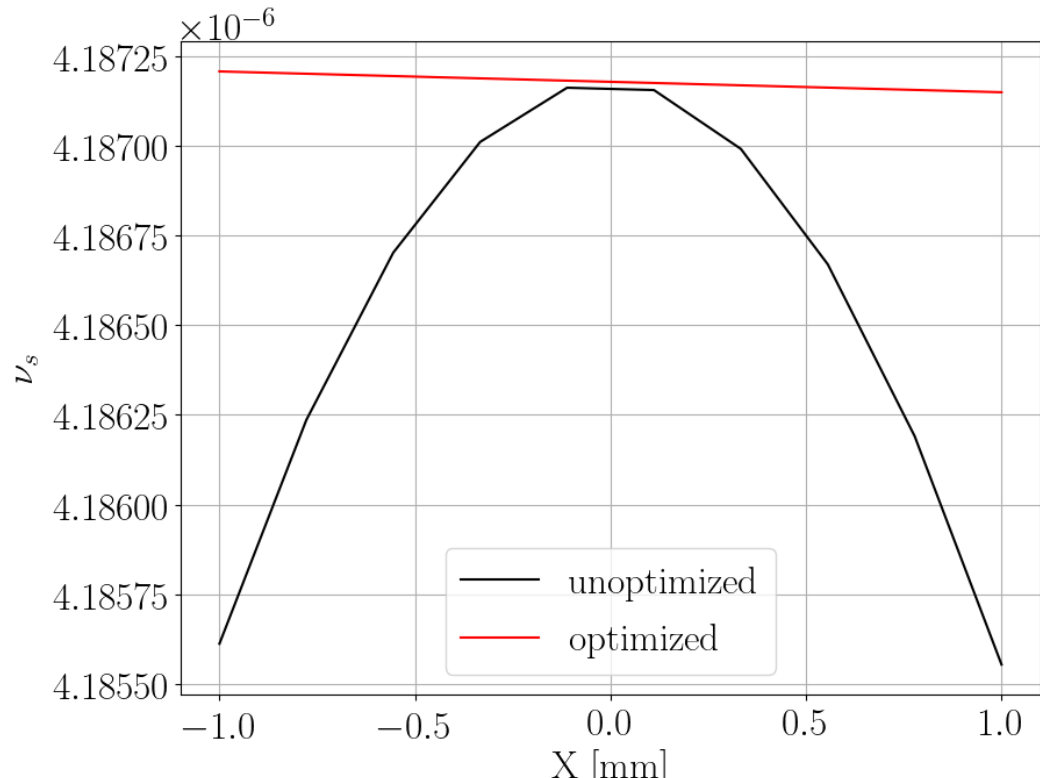
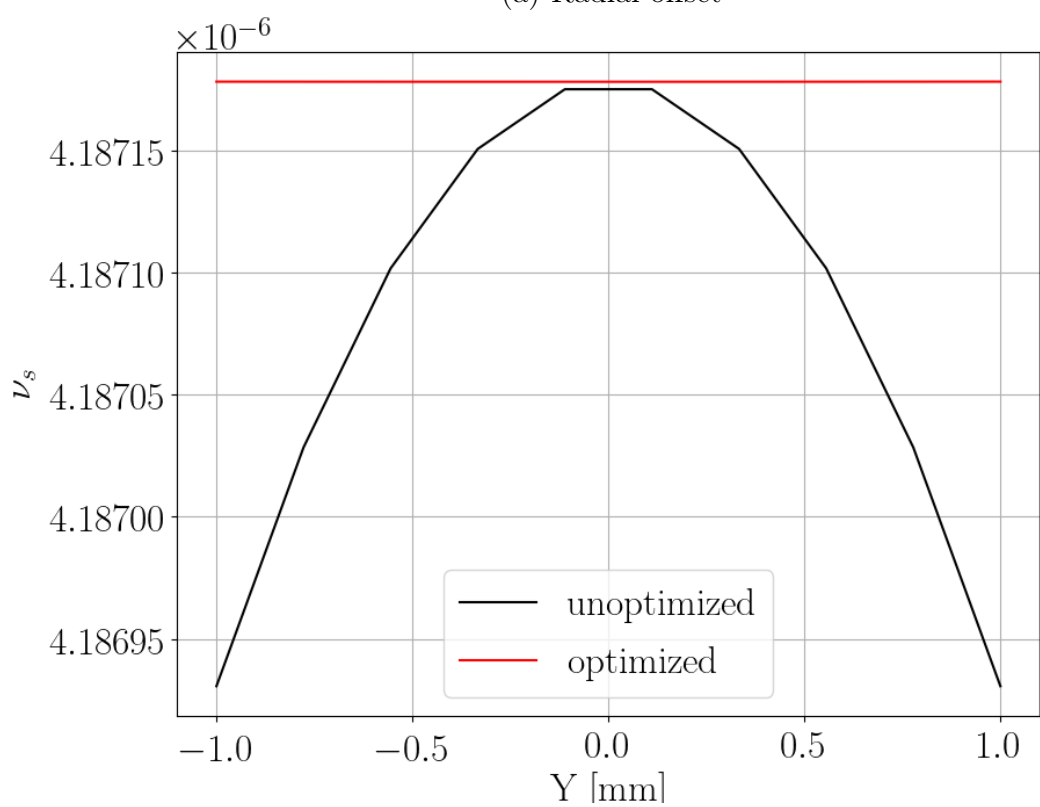


Рис. 1.2: Standard deviation vs spin wheel roll rate.



(a) Radial offset



(b) Vertical offset

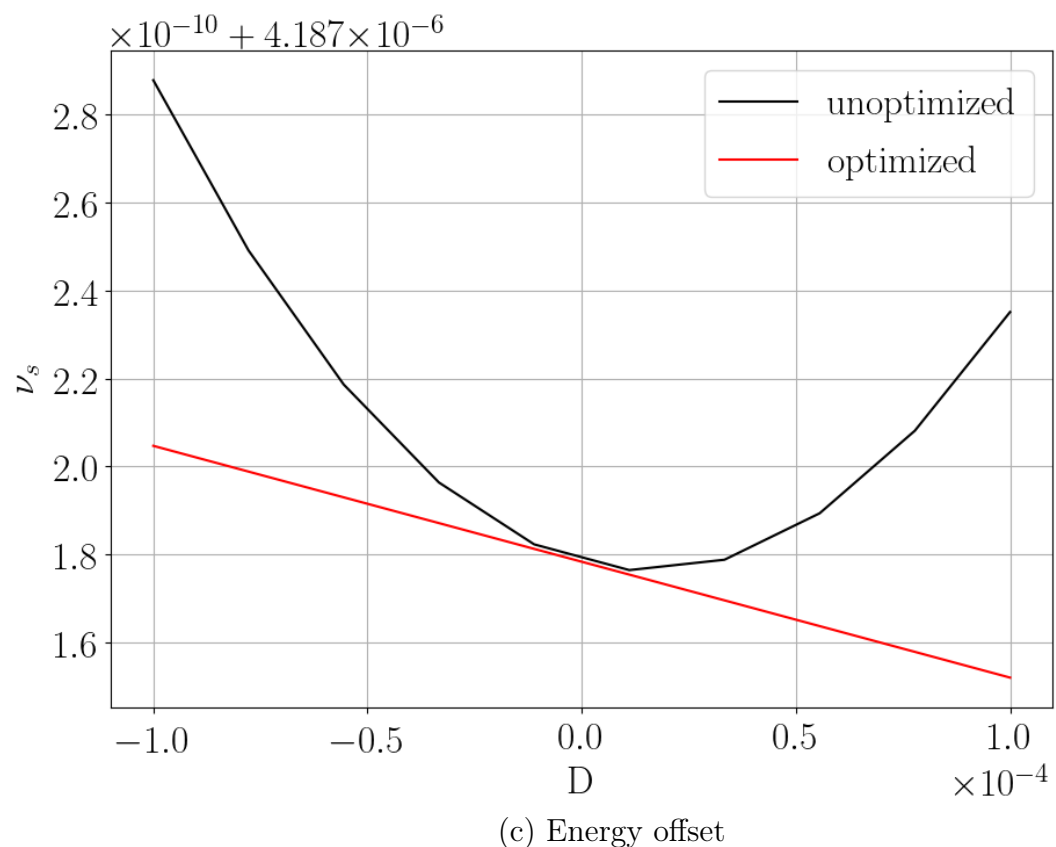


Рис. 1.3: The dependence of a particle spin tune on its initial offset from the reference particle.

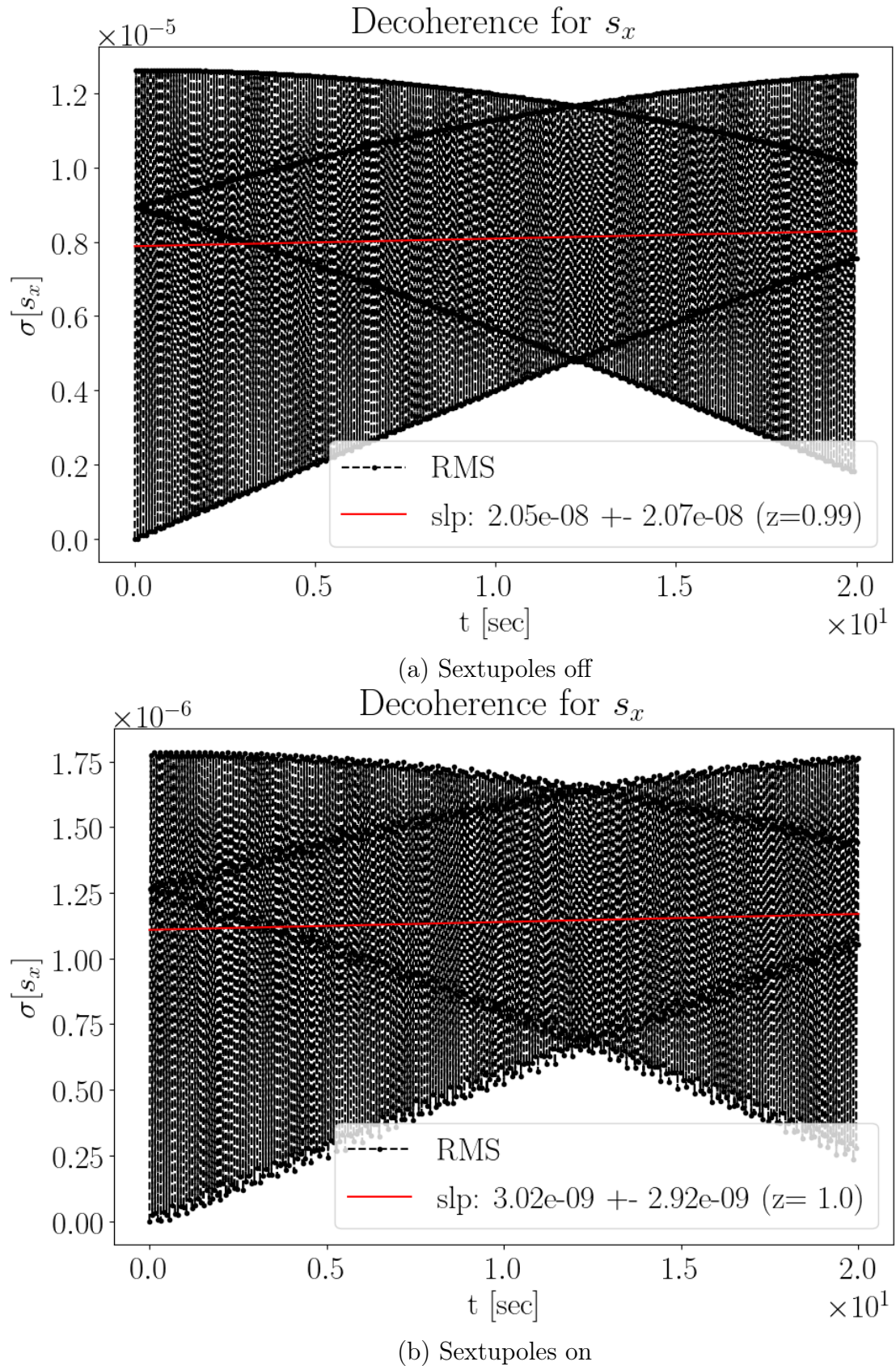


Рис. 1.4: Standard deviation of the radial spin vector component distribution in a bunch.

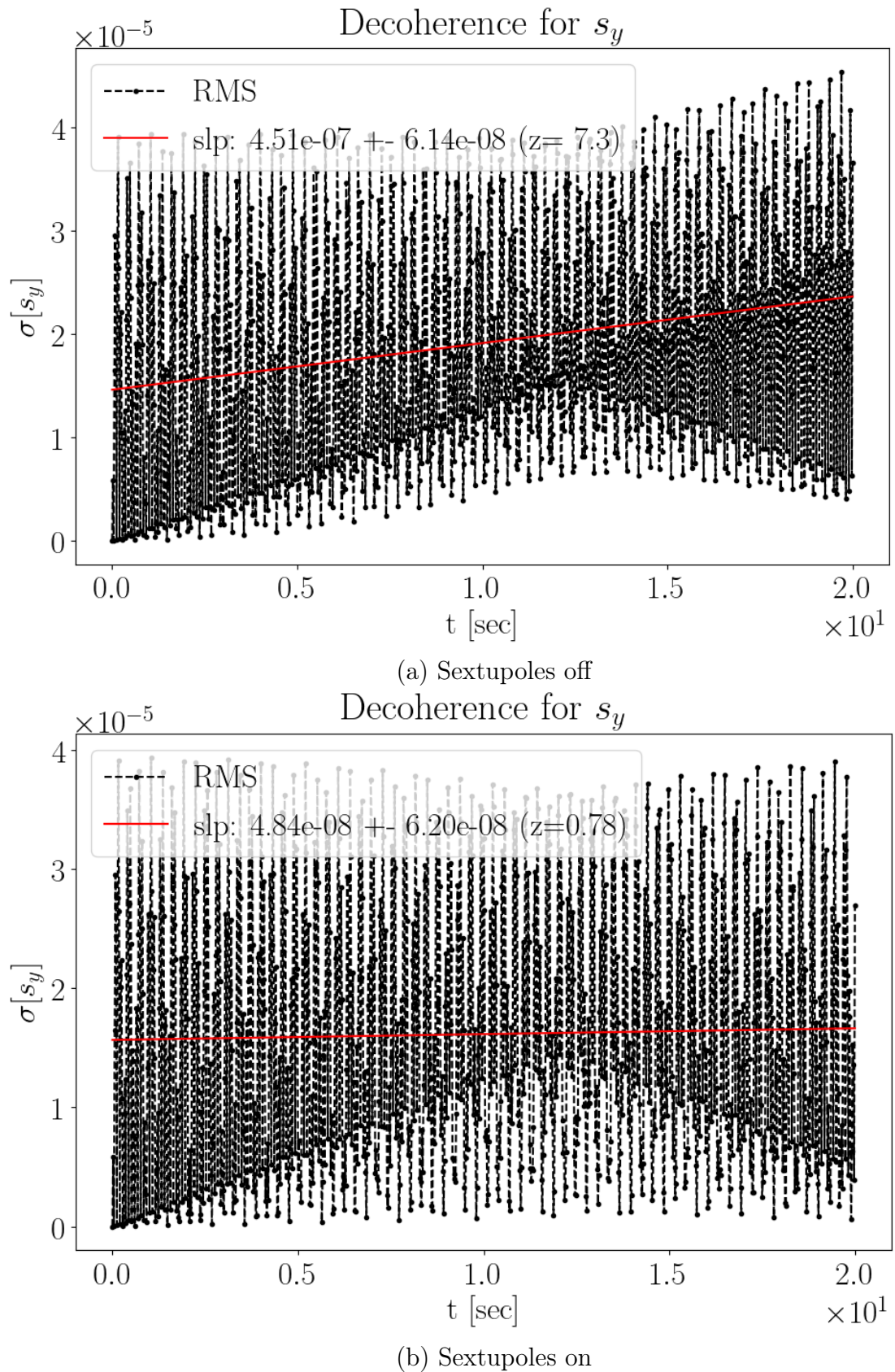


Рис. 1.5: Standard deviation of the radial spin vector component distribution in a bunch.

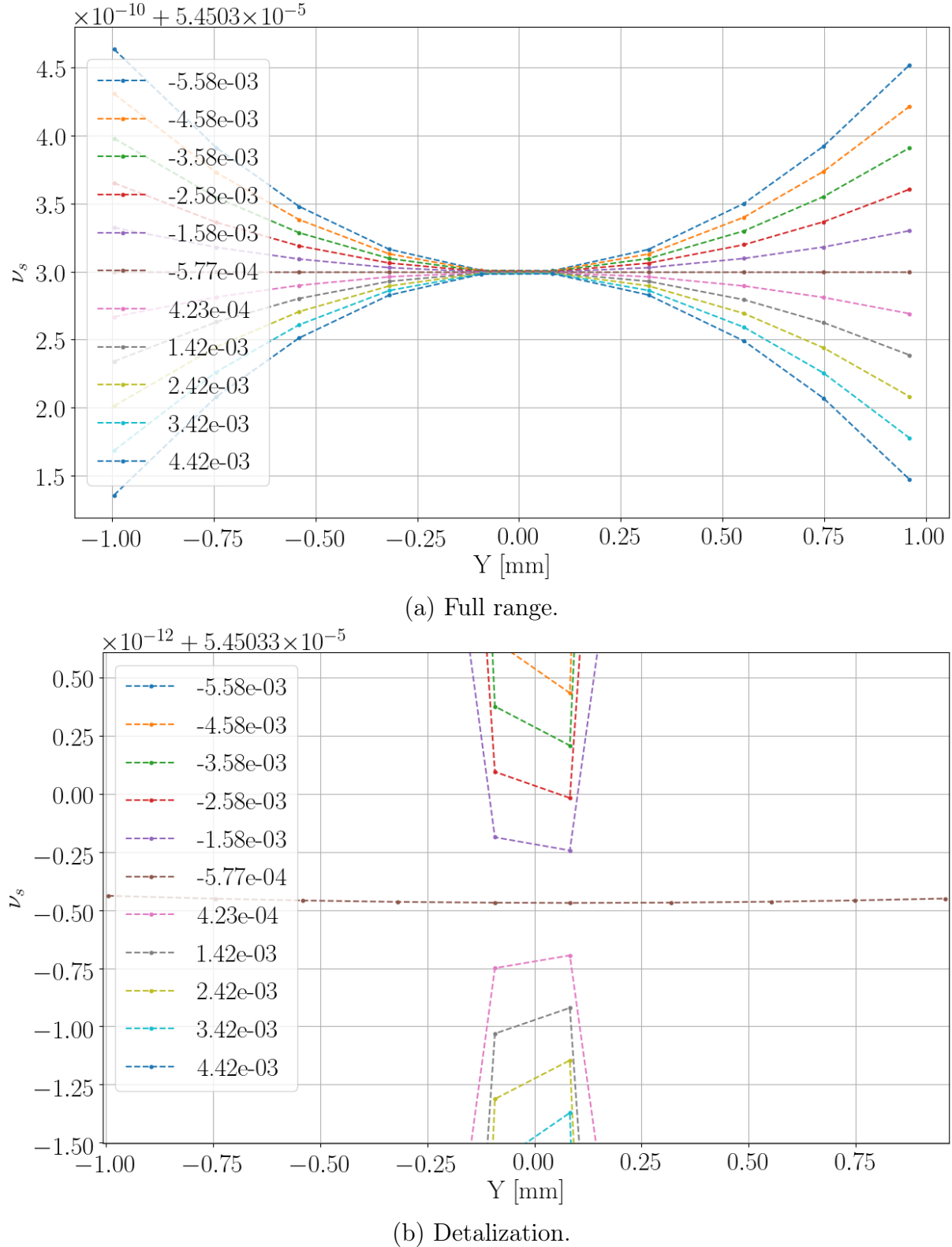


Рис. 1.6: Spin tune ν_s as a function of the particle's vertical offset from the closed orbit. Color marks different G_Y values.

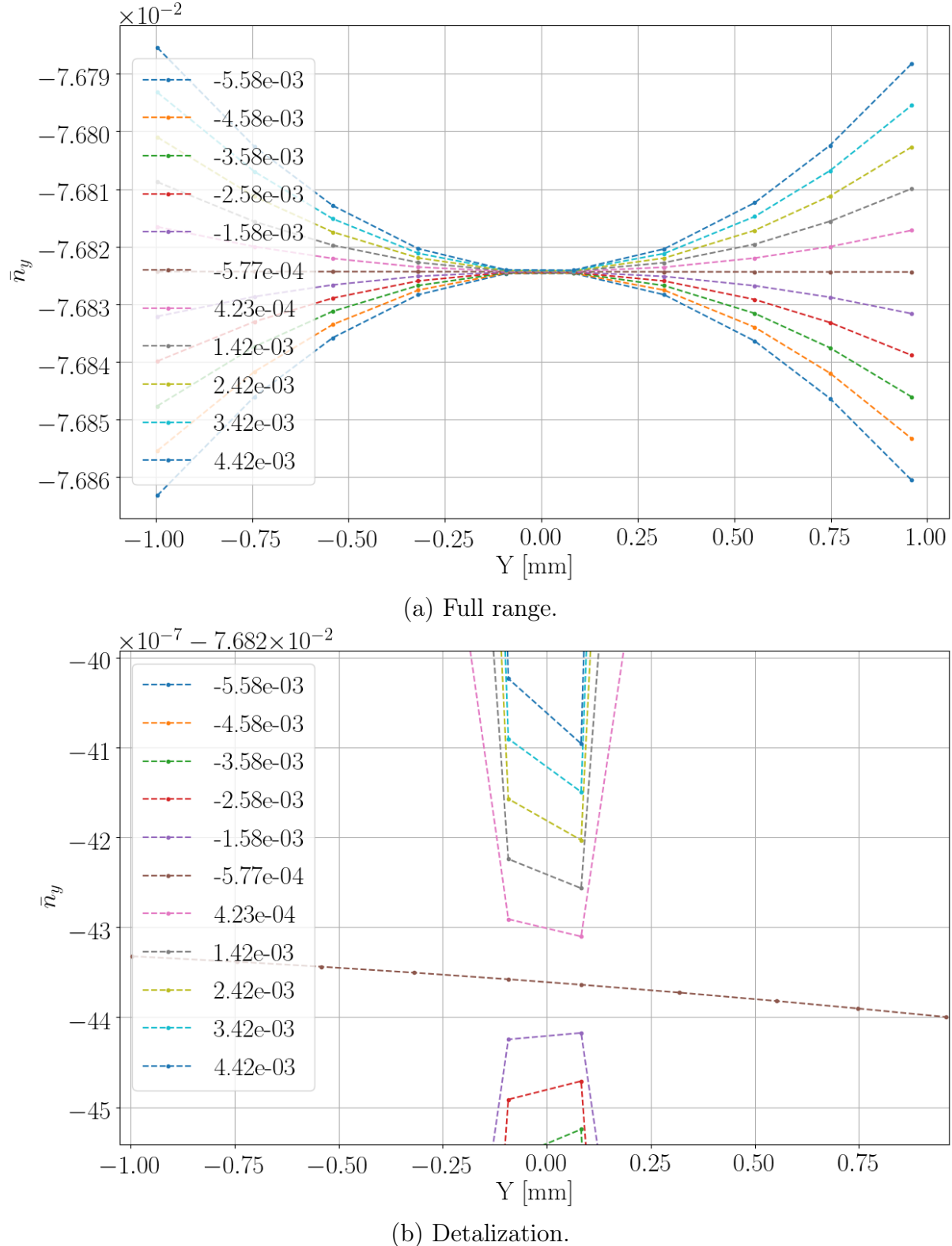


Рис. 1.7: Vertical component \bar{n}_y of the invariant spin axis as a function of the particle's vertical offset from the closed orbit. Color marks different G_Y values

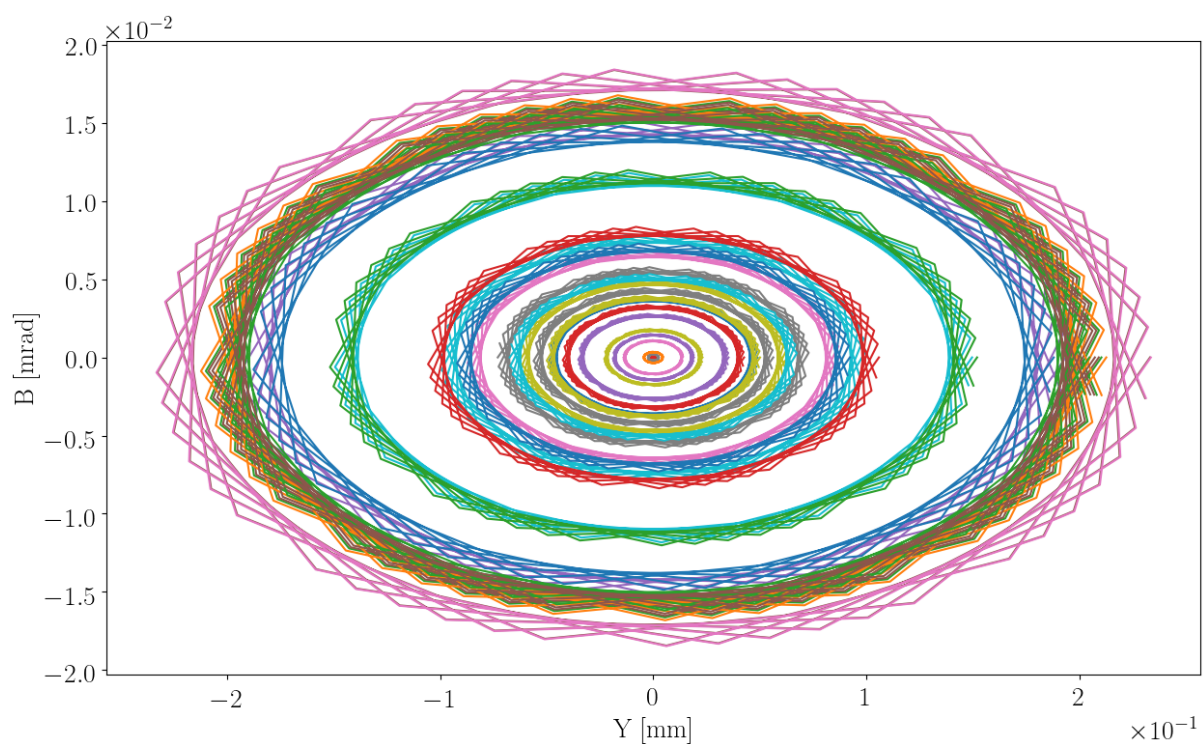


Рис. 1.8: Particle trajectories in the (Y, B) phase space.

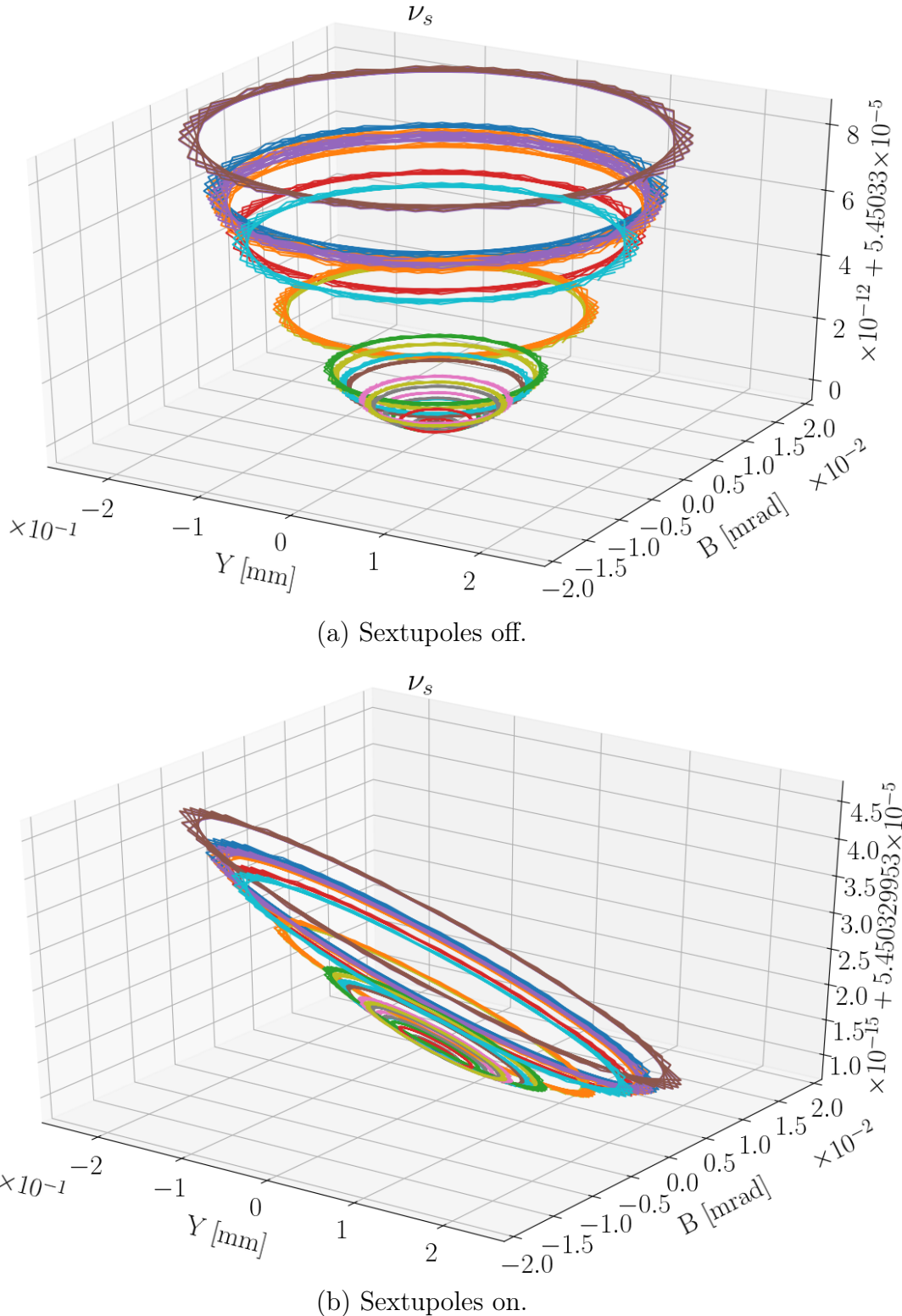


Рис. 1.9: Particle spin tunes computed at their trajectories in an imperfect FS lattice.

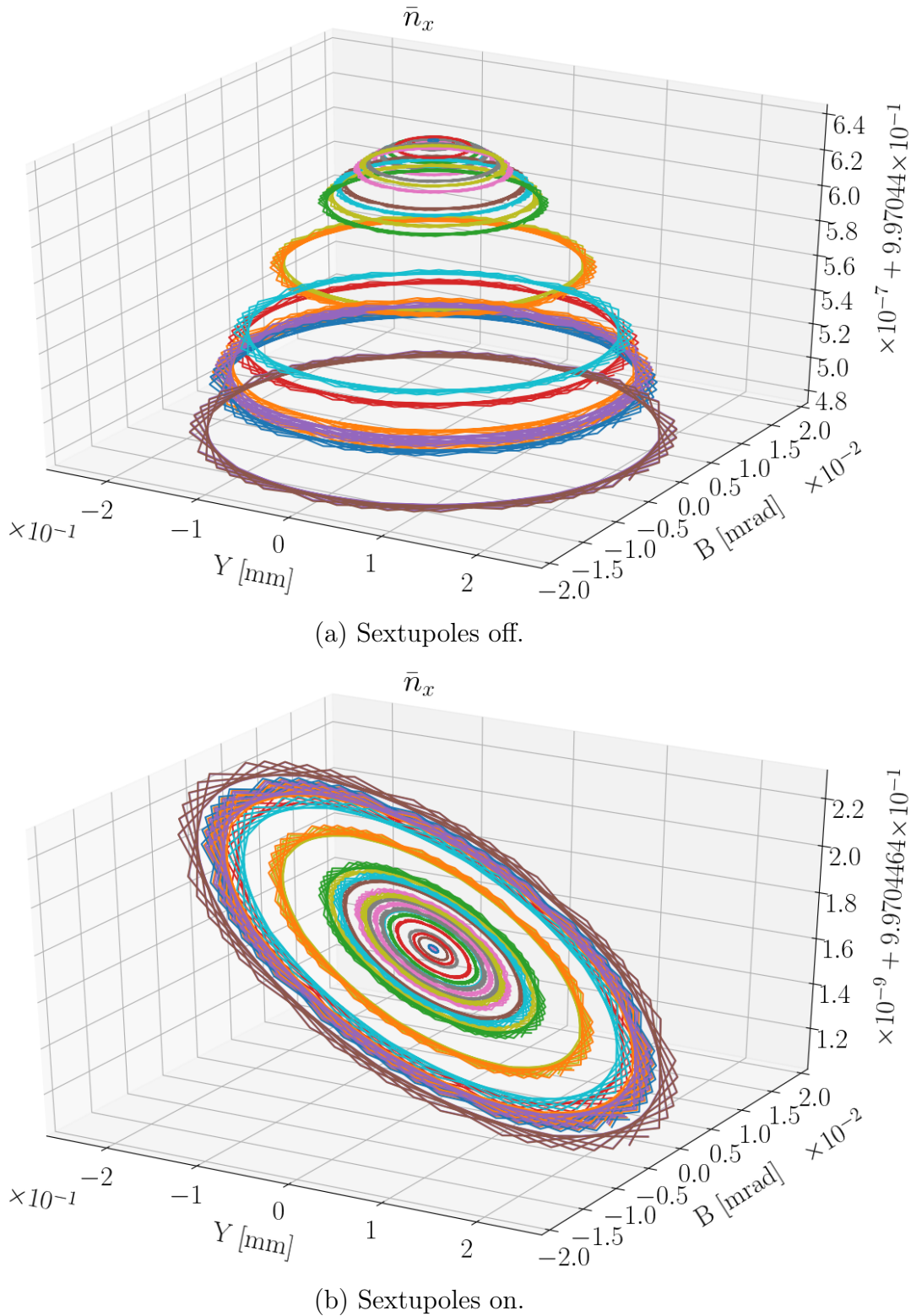


Рис. 1.10: Particle's radial ISA components computed at their trajectories in an imperfect FS lattice.

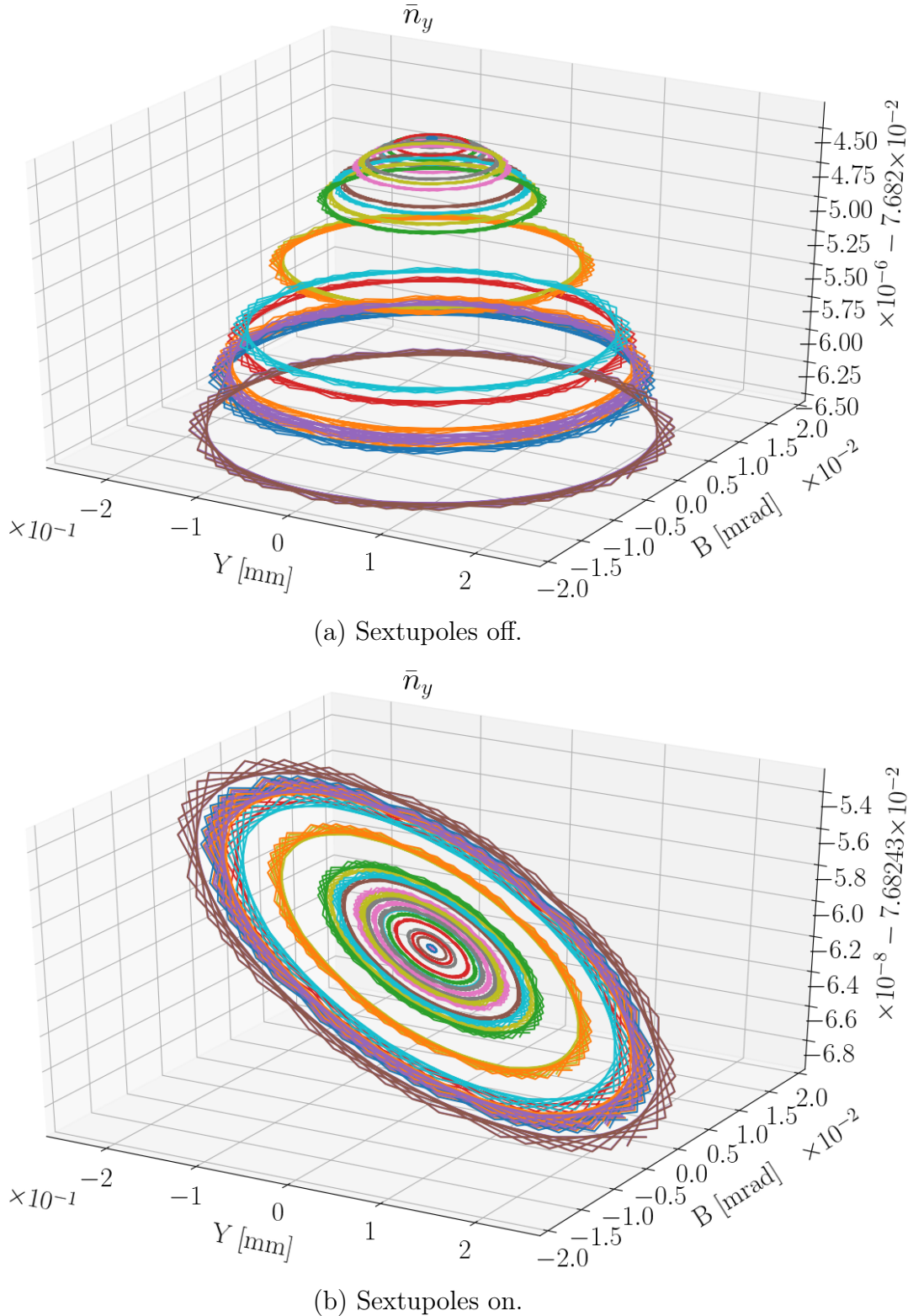


Рис. 1.11: Particle's vertical ISA components computed at their trajectories in an imperfect FS lattice.

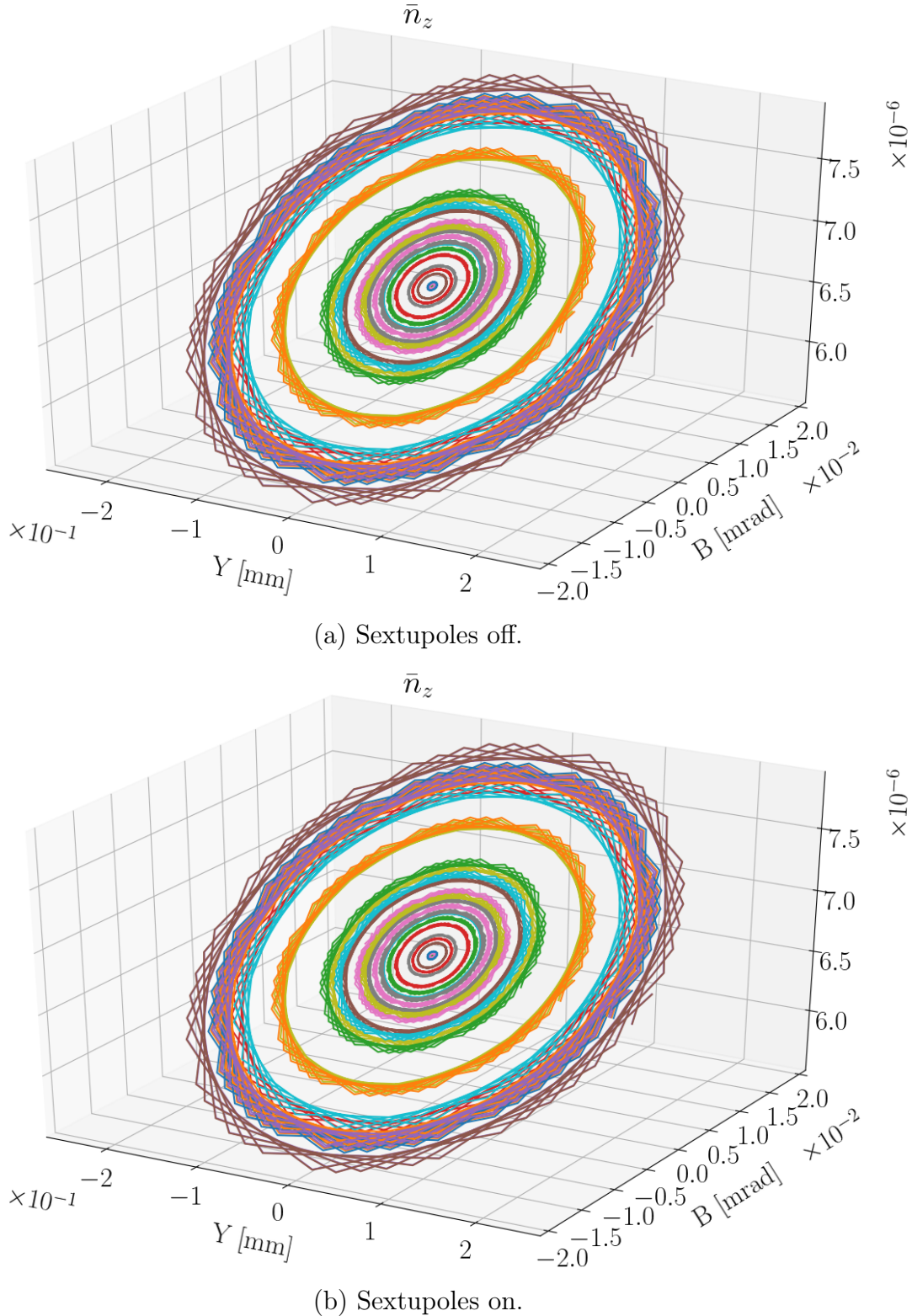


Рис. 1.12: Particle's longitudinal ISA components computed at their trajectories in an imperfect FS lattice.

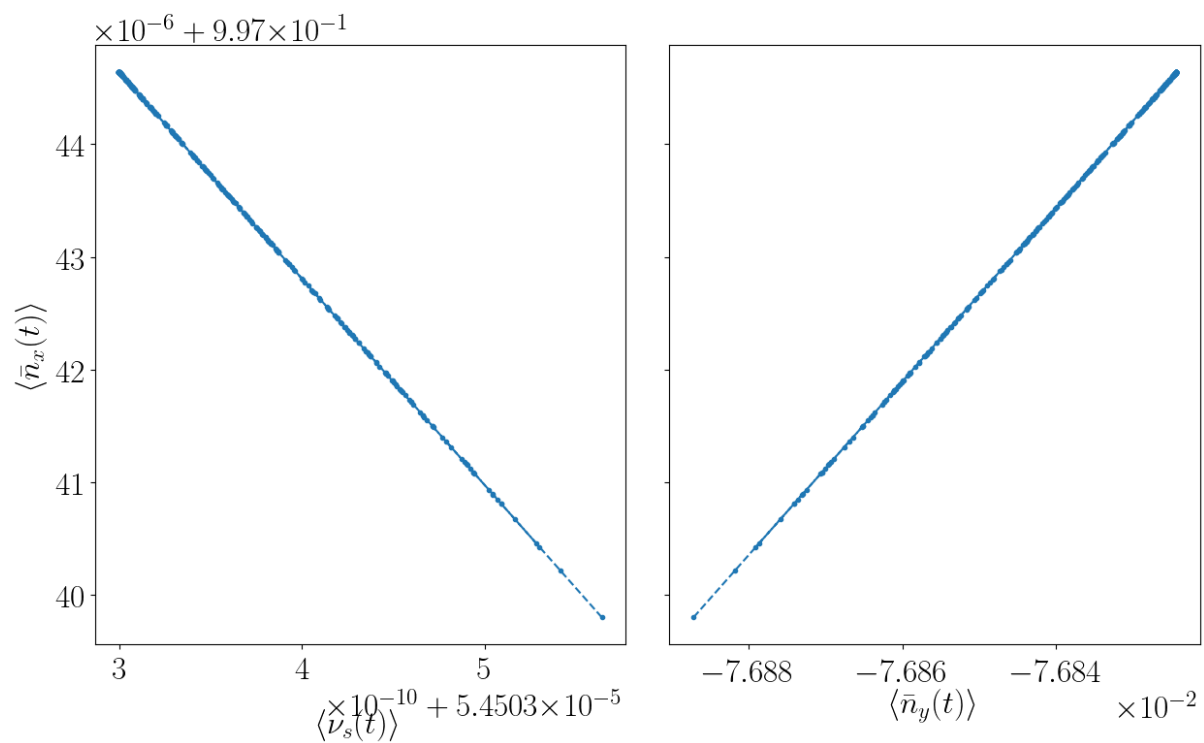


Рис. 1.13: Mean level of the radial and vertical ISA components versus the corresponding value of spin tune.

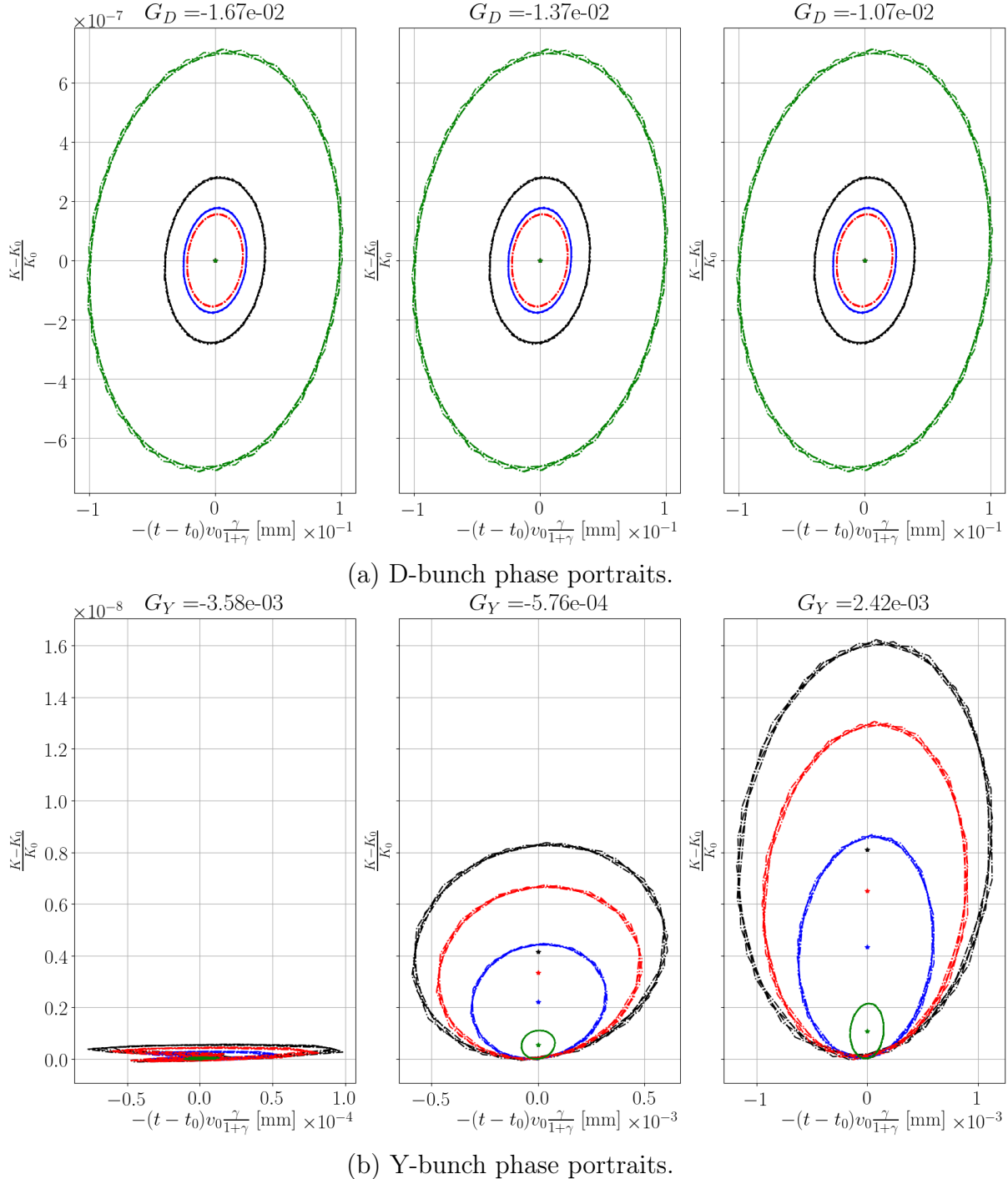
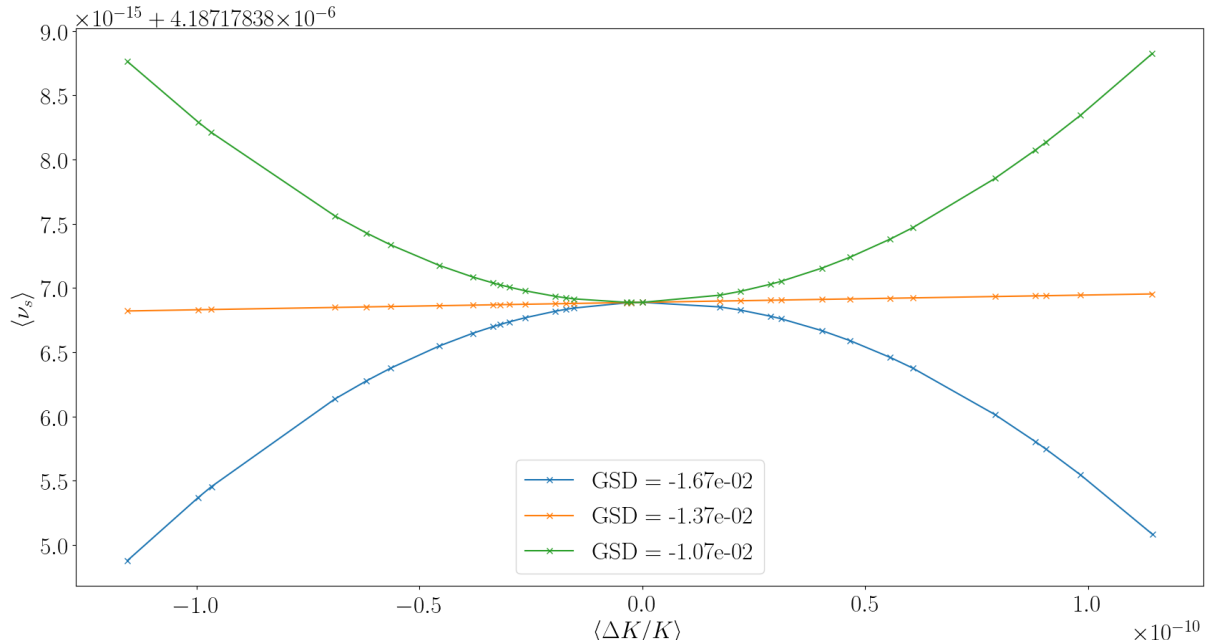
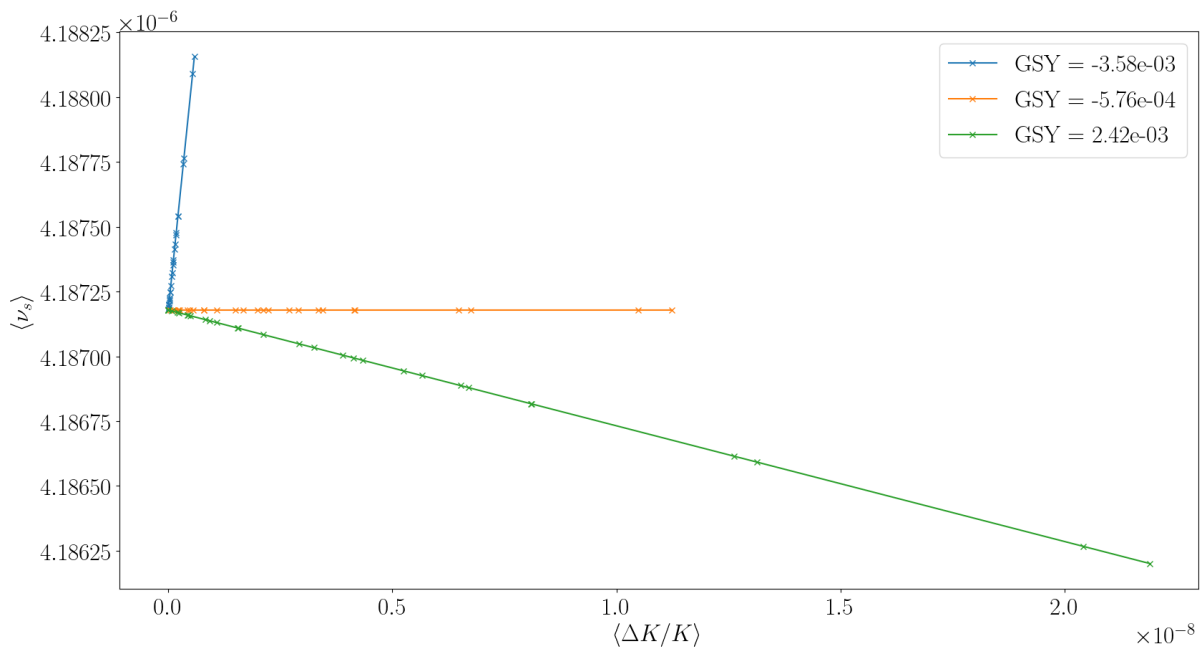


Рис. 1.14: Longitudinal phase space particle portraits. Asterisks mark the ellipse centers. Colors mark trajectories of particles with differing initial vertical offset from the reference orbit.

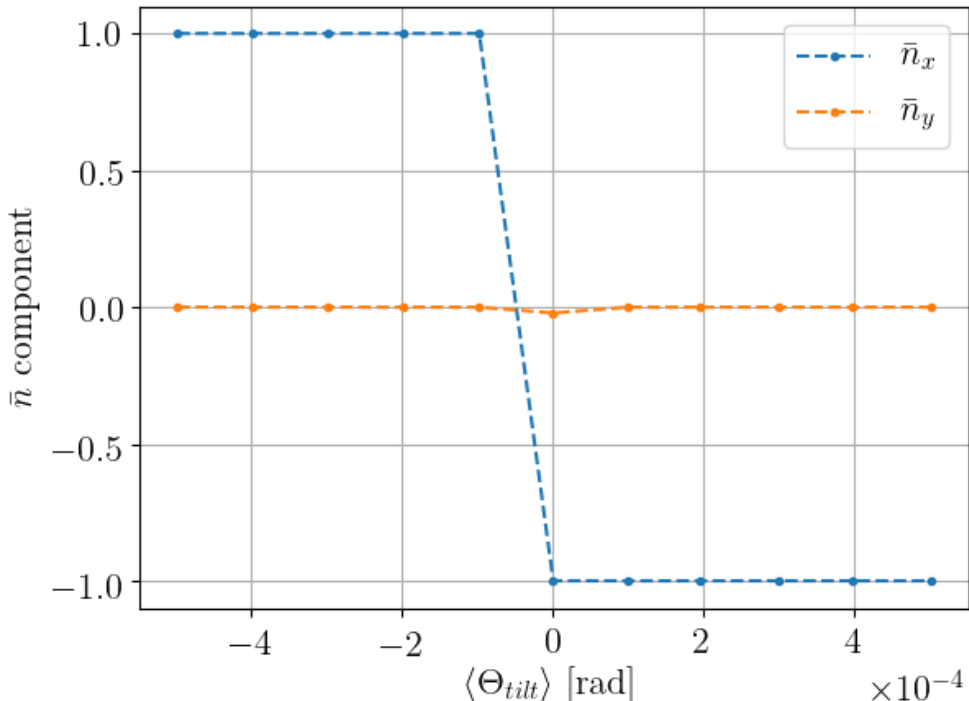


(a) For the D-bunch.

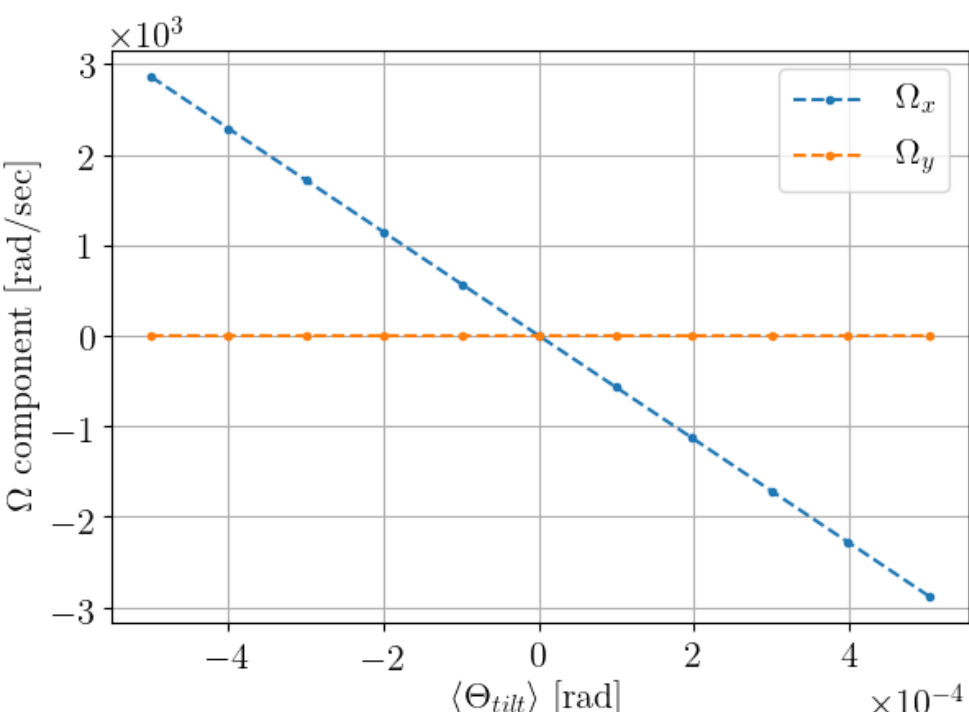


(b) For the Y-bunch.

Рис. 1.15: Particle mean spin tune level as a function of its equilibrium level energy at different sextupole strengths.

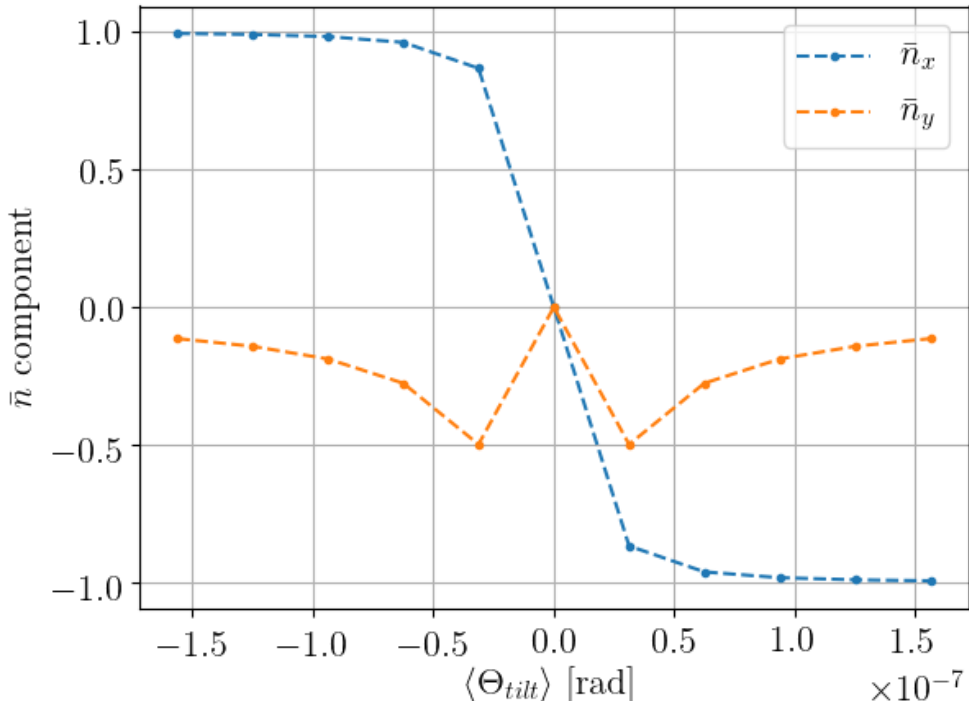


(a) Spin precession axis \bar{n} components.

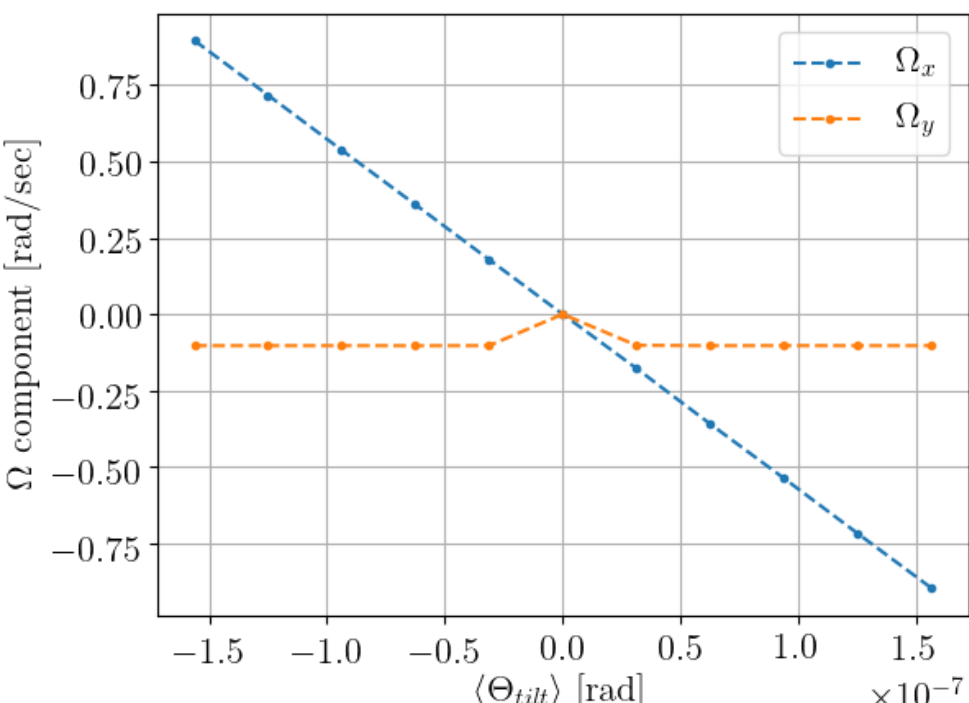


(b) Angular velocity Ω components.

Рис. 1.16: Reference particle's spin precession axis and angular velocity components as functions of the mean E+B element tilt angle. Element tilts are normally distributed. Color identifies the component; radial (blue) and vertical (orange).

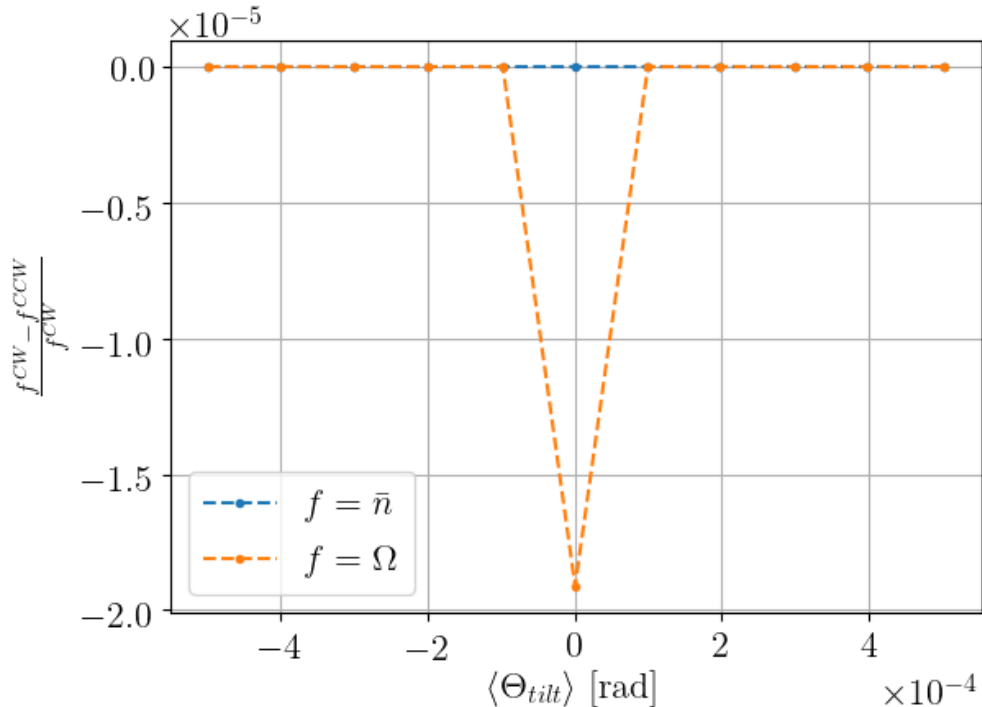


(a) Spin precession axis \bar{n} components.

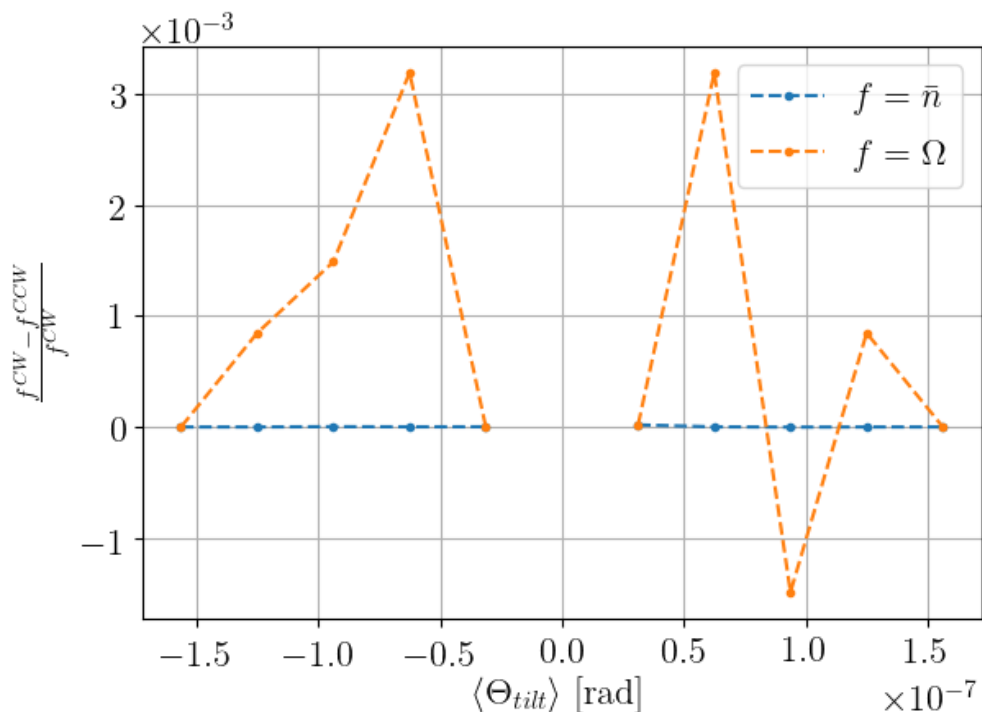


(b) Angular velocity vector Ω components.

Рис. 1.17: Reference particle's spin precession axis and angular velocity components as functions of the mean E+B element tilt angle. Three mutually-compensated tilt pairs plus an uncompensated rotation. Color identifies the component; radial (blue) and vertical (orange)



(a) Normally distributed E+B element tilts.



(b) Mutually-compensated element tilts.

Рис. 1.18: Relative difference between the CW and CCW beams' spin precession axis and angular velocity radial components. Color marks the compared variable: spin precession axis (blue) and angular velocity (orange).

Литература

- [1] Shatunov YM. Polarized beams in accelerators and storage rings. Novosibirks, Russia: SB RAS press; 2015.
- [2] Senichev Y, Andrianov S, Ivanov A, Chekmenev S, 3tin Berz, Valetov E. INVESTIGATION OF LATTICE FOR DEUTERON EDM RING. In: Modeling of current and future machnies. Shanghai, China; 2015. Available from: <http://accelconf.web.cern.ch/AccelConf/ICAP2015/papers/modbc4.pdf>.
- [3] Koop IA. Asymmetric energy colliding ion beams in the EDM storage ring. In: Beam Dynamics and Electromagnetic Fields. Shanghai, China; 2013. p. 1961–1963. Available from: <http://accelconf.web.cern.ch/accelconf/ipac2013/papers/tupwo040.pdf>.
- [4] Berz M, Makino K. COSY Infinity website. 220 Trowbridge Rd, East Lansing, MI 48824, USA;. Available from: cosyinfinity.org.
- [5] Berz M, Makino K. COSY INFINITY 10.0 Beam Physics Manual. 220 Trowbridge Rd, East Lansing, MI 48824, USA; 2017.
- [6] Valetov E. FIELD MODELING, SYMPLECTIC TRACKING, AND SPIN DECOHERENCE FOR EDM AND MUON G-2 LATTICES. Michigan State University. Michigan, USA;,. Available from: http://collaborations.fz-juelich.de/ikp/jedi/public_files/theses/valetovphd.pdf.
- [7] Anastassopoulos D, Anastassopoulos V, Babusci D, et al. AGS Proposal: Search for a permanent electric dipole moment of the

- deuteron nucleus at the 10^{-29} e· cm level. BNL; 2008. Available from: https://www.bnl.gov/edm/files/pdf/deuteron_proposal_080423_final.pdf.
- [8] Senichev Y, Zyuzin D. SPIN TUNE DECOHERENCE EFFECTS IN ELECTRO- AND MAGNETOSTATIC STRUCTURES. In: Beam Dynamics and Electromagnetic Fields. vol. 5. Shanghai, China: JACoW; 2013. p. 2579–2581. OCLC: 868251790. Available from: <https://accelconf.web.cern.ch/accelconf/IPAC2013/papers/wepea036.pdf>.
 - [9] Berz M, Makino K. COSY INFINITY 10.0 Programmer's manual. 220 Trowbridge Rd, East Lansing, MI 48824, USA; 2017.
 - [10] Senichev Y, Aksentev A, Ivanov A, Valegov E. Frequency domain method of the search for the deuteron electric dipole moment in a storage ring with imperfections. arXiv:171106512 [physics]. 2017 11;ArXiv: 1711.06512. Available from: <http://arxiv.org/abs/1711.06512>.
 - [11] Saleev A, Nikolaev NN, Rathmann F, et al. Spin tune mapping as a novel tool to probe the spin dynamics in storage rings. Phys Rev Accel Beams. 2017 7;20:072801. Available from: <https://link.aps.org/doi/10.1103/PhysRevAccelBeams.20.072801>.